π-band contribution to the optical properties of carbon nanotubes: Effects of chirality

Shuichi Tasaki

Department of Physics, Nara Women's University, Kita-Uoya-Nishi-machi, Nara 630, Japan
and Institute for Fundamental Chemistry, 34-4 Takano Nishihiraki-cho, Sakyo-ku, Kyoto 606, Japan

Koji Maekawa*

Institute for Fundamental Chemistry, 34-4 Takano Nishihiraki-cho, Sakyo-ku, Kyoto 606, Japan

Tokio Yamabe

Division of Molecular Engineering, Faculty of Engineering, Kyoto University, Sakyo-ku, Kyoto 606-01, Japan
and Institute for Fundamental Chemistry, 34-4 Takano Nishihiraki-cho, Sakyo-ku, Kyoto 606, Japan
(Received 16 October 1997)

We study the π-band contribution to the optical properties of the carbon nanotubes based on the tight-binding model, including optical absorptions, optical rotatory power, and circular dichroism. By taking into account not only the interband contributions but also the free-carrier contributions, the dielectric functions and the third-rank tensor responsible for the optical activity are calculated. The following have been shown. (i) The features of the dielectric functions are consistent with the ellipsometry experiments by de Heer and co-workers [Science **268**, 845 (1995)]; (ii) The calculated plasma frequency is of the same order of magnitude as the one recently observed by Bommeli *et al.* [Solid State Commun. **99**, 513 (1996)]. (iii) Chiral nanotubes are, as expected, optically active and the spectra of their optical rotatory power (RP) and circular dichroism (CD) are highly oscillatory. (iv) Nanotubes with a diameter about 4 nm can give RP and CD that are of the same order of magnitude as those of certain organic compounds. (v) The RP and CD decrease as the diameter increases. [S0163-1829(98)06608-9]

I. INTRODUCTION

Since their discovery[1] by Iijima, carbon nanotubes have been intensively studied both experimentally[2–8] and theoretically.[9–24] Nanotubes consist of coaxial cylinders of graphene sheets, the number of sheets ranging from 1 to 50. They are predicted to be metallic or semiconducting depending on the structure, mainly the way of connection of carbon atoms.[9–15] It is also predicted that their geometry gives rise to interesting properties. Due to the cylindrical shape, a uniform magnetic field along the tubule axis causes the Aharonov-Bohm effect,[15–18] which can be observed as an oscillation of the magnetic susceptibility as a function of the external magnetic field or as a magnetic-field-induced shift of optical absorption edges. The Peierls instability[11,12,21,22] is expected because of the quasi-one-dimensionality. On the other hand, the chirality due to the spiral alignment, which is one of the main features of the nanotube geometry, and its consequence are not investigated so well. Since one of the consequences of chirality is the optical activity, we study the optical properties of nanotubes including the optical rotatory power and circular dichroism.

Experimentally, optical properties of nanotubes have been studied by the optical ellipsometry[6] or by the electron-energy-loss spectroscopy (EELS).[7] More recently, Bommeli *et al.*[8] reported the reflectivity measurements of aligned nanotubes, particularly paying attention to the free-carrier (Drude) contributions. Theoretically, Ajiki and Ando[18] studied the low-energy optical absorption due to the interband transitions as a probe of the Aharonov-Bohm effect. Lin and Shung[19] reported the frequency dependence of the dielectric functions due to π bands within the gradient approximation and investigated a low-energy peak of EELS. Mintmire and White[20] calculated the dielectric functions using a first-principles local-density-functional method and taking into account both π- and σ-band contributions.

The energy bands of a nanotube, as a rolled graphite sheet, consist of the ones originated from the π orbits (π bands) and the ones from the σ orbits (σ bands) and, according to the band calculation of the graphite sheet[25] and zigzag nanotubes,[11] there exists a threshold energy of 6–10 eV, below which only the π-π transitions are allowed. Hence we focus our attention on the response of light with energy up to this threshold so that the π-π transitions give a dominant contribution.

In the rest of this section the electronic property of the π bands of nanotubes is briefly reviewed. In Sec. II we calculate the response functions to a monochromatic electromagnetic field (i.e., the dielectric function and third-rank tensor responsible for the optical activity) with the aid of the linear-response theory. Then we find the following relation between the electric displacement $\mathbf{D}(\mathbf{k},\omega)$ and the electric field $\mathbf{E}(\mathbf{k},\omega)$ for the components with wave vector $\mathbf{k}$ and frequency ω:

$$\mathbf{D}(\mathbf{k},\omega) = \epsilon_\parallel [\mathbf{E}(\mathbf{k},\omega) \cdot \mathbf{e}_z]\mathbf{e}_z + \epsilon_\perp \{\mathbf{E}(\mathbf{k},\omega) - [\mathbf{E}(\mathbf{k},\omega) \cdot \mathbf{e}_z]\mathbf{e}_z\}$$
$$+ i\gamma_\parallel \{[\mathbf{k} \times \mathbf{E}(\mathbf{k},\omega)] \cdot \mathbf{e}_z\}\mathbf{e}_z + i\gamma_\perp^{(1)}[\mathbf{e}_z \cdot \mathbf{E}(\mathbf{k},\omega)]$$
$$\times (\mathbf{e}_z \times \mathbf{k}) + i\gamma_\perp^{(2)}\{\mathbf{e}_z \times [\mathbf{k} \times \mathbf{E}(\mathbf{k},\omega)]\},$$

where $\mathbf{e}_z$ is the unit vector along the tubule axis, $\epsilon_\parallel$ and $\epsilon_\perp$ are the dielectric functions, and $\gamma_\parallel$, $\gamma_\perp^{(1)}$, and $\gamma_\perp^{(2)}$ are related to the optical activity. In Sec. III the frequency dependences

of the dielectric functions $\epsilon_\parallel$ and $\epsilon_\perp$ are investigated and compared with previous works.[18–20] Our results agree well with the previous ones. Then, by using a very short relaxation time, we simulate the dielectric functions for a bundle of nanotubes, which qualitatively explain the difference between the observed parallel and perpendicular dielectric functions with respect to the sample axis.[6] Also, for large nanotubes, the square of the plasma frequency is shown to be proportional to the carbon density ρ_C and inversely proportional to the tubule diameter D. The experimental value of the plasma frequency (0.215 eV) obtained from the data by Bommeli et al.[8] is of the same order of magnitude as, but smaller by a factor of $\sim \frac{1}{3}$ than, the calculated one (0.686 eV) for a sample of randomly synthesized multilayer nanotubes with the outermost diameter $D_{ex} \simeq 11$ nm and the hollow diameter $D_{in} \simeq 2.2$ nm. In Sec. IV the optical activity of the ensemble of nanotubes is considered and the difference $\gamma_\parallel - \gamma_\perp^{(1)}$ is shown to be related to the optical rotatory power and circular dichroism. It shows negative and positive Cotton effects alternately as the frequency increases. The low-frequency peaks of the optical activity are suppressed, which indicates the achiral nature of the electronic states near the Fermi points. We have also found that the magnitude of the circular dichroism for nanotubes with diameter about 4 nm and density 30% of the graphite crystal is of the same order of magnitude as those observed in certain organic compounds.[26] Since the infinitely large nanotube is the achiral two-dimensional (2D) graphite, the optical activity diminishes when the diameter becomes larger. Section V is devoted to the summary and concluding remarks. Details of the calculations of response functions are shown in Appendix A–C. Particularly, in Appendix B we show the explicit expressions of the response functions valid for a more general case where each carbon atom is described by j atomic-centered basis functions.

The structure of a nanotube, as a rolled graphite sheet, is specified by the way of rolling, i.e., by the relative lattice vector $\mathbf{R}_{ab} = a\mathbf{x} + b\mathbf{y}$ between two hexagons to be identified, where a and b are integers and $\mathbf{x}$ and $\mathbf{y}$ are two unit vectors of the two-dimensional graphite lattice[24,27] (Fig. 1). In the discussions of the band structure,[10,11] usually the index is confined so that the angle θ_{ab} of $\mathbf{R}_{ab}$ with respect to a given
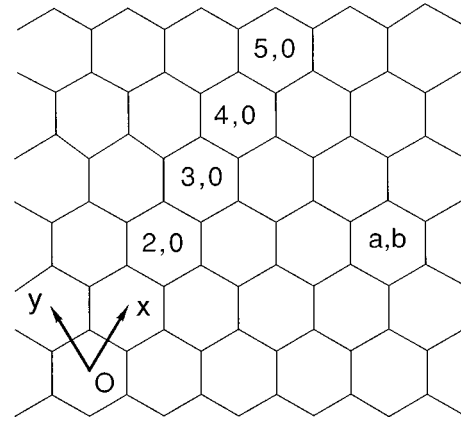

FIG. 1. Parametrization of nanotubes. Vectors $\mathbf{x}$ and $\mathbf{y}$ stand for the unit vectors of the graphite lattice. The nanotube (a,b) is formed by rolling the graphite sheet from the front to the back so that the hexagon at O is overlapped with the hexagon (a,b).

direction is in between 0 and $\pi/6$ and the chirality of the nanotube is specified by the type of rolling (i.e., from the back of the sheet to the front or from the front to the back). Instead, once we fix the way of rolling the sheet (e.g., from the front to the back), we can uniquely specify the structures of nanotubes by the vector $\mathbf{R}_{ab}$ with $-\pi/6 \leq \theta_{ab} \leq \pi/6$. Here we use a tubule index (a,b) satisfying $a \geq 1$ and $-a+1 \leq b \leq 0$. Then the mirror image of the nanotube (a,b) is $(a,0)$ for $b=0$ and $(a,-a-b)$ for $b \neq 0$. Hence the achiral nanotube (a,b) is characterized by $b=0$ or $a+2b=0$ with $b \neq 0$.

The π bands of the nanotube are well described by the tight-binding model.[9–11] Its Hamiltonian is given by

$$H = -t_0 \sum_{i,j;\sigma} \{C_{i\sigma}^\dagger C_{j\sigma} + \text{H.c.}\},$$

where $C_{i\sigma}$ and $C_{i\sigma}^\dagger$ are annihilation and creation operators of a π electron with spin σ at the ith site, t_0 is the hopping energy, and the sum runs over the nearest-neighbor pairs. The Hamiltonian H gives, for the nanotube (a,b), a one-dimensional (1D) bands[9,11,19,24,27]

$$E_\pm(N,k) = \pm t_0 \sqrt{1 + 4\cos\left(\frac{2\pi N}{a} - \frac{a+2b}{2a}k\ell\right)\cos\frac{k\ell}{2} + 4\cos^2\frac{k\ell}{2}}, \tag{1.1}$$

where ℓ is $\frac{3}{2}$ times the interatomic distance, $N = 0,1,\ldots,a-1$, and $-\pi/\ell \leq k \leq \pi/\ell$. The plus and minus subscripts stand for the conduction and valence band, respectively.

Equation (1.1) predicts the following. A nanotube (a,b) is a metal when $2a+b=3n$ (n an integer) and generally has four metallic bands with energies $E_\pm(n,k)$ (Fermi wave number $k = k_F = 2\pi/3\ell$) and $E_\pm(a-n,k)$ (Fermi wave number $k = -k_F = -2\pi/3\ell$). When $2a+b=3n$ and $n=a-n$, the nanotube has only two metallic bands and is achiral because of $a+2b=0$. Strictly speaking, this is not true except

for $n=-b$ since expression (1.1) does not include the effects of curvature on the electronic structure.[10,11,14] However, the energy gaps for nanotubes with $2a+b=3n$ ($n \neq -b$) are small [less than 10 meV (Refs. 10 and 11)] even for a small nanotube with a diameter of 1 nm, which is negligible at room temperature. Also, as will be seen in Sec. III, the band structure[20] calculated by the local-density-functional method agrees well with Eq. (1.1) at energy less than about 3 eV even for a very small nanotube (diameter $\simeq 0.7$ nm). Clearly the effects of curvature diminishes as the tubule diameter

increases and hence at energy less than 5 eV, they are expected to be negligibly small for nanotubes with a diameter more than a few nanometers at room temperature. Note that when $2a+b$ is not divisible by 3, a nanotube (a,b) is a semiconductor.

II. OPTICAL RESPONSE FUNCTIONS

The electromagnetic response to the weak applied field is fully characterized by the dielectric function $\bar{\epsilon}_{ij}(\mathbf{k},\omega)$, depending on the frequency ω and wave vector $\mathbf{k}$, and the optical processes such as absorption and diffraction are well described by its long-wavelength limit[28] $\epsilon_{ij}\equiv\bar{\epsilon}_{ij}(\mathbf{0},\omega)$. However, in order to take into account the optical activity, we need to consider $\mathbf{k}$-linear terms of $\bar{\epsilon}_{ij}(\mathbf{k},\omega)$ as they may have different symmetry from the $\mathbf{k}$-independent ones.[28]

The dielectric function ϵ_{ij} is given by[29-31,18,19]

$$\epsilon_{ij}=\delta_{ij}+\frac{8\pi e^2\hbar}{m^2\omega}\rho_T\sum_{\tau,\tau'=\pm}\sum_{N,N'}\int dk$$
$$\times\int dk'\frac{\langle N'k'\tau'|\hat{p}_i|Nk\tau\rangle\langle Nk\tau|\hat{p}_j|N'k'\tau'\rangle}{E_{\tau'}(N',k')-E_\tau(N,k)+\hbar\omega+i0}$$
$$\times\frac{f(E_{\tau'}(N',k'))-f(E_\tau(N,k))}{E_{\tau'}(N',k')-E_\tau(N,k)},\qquad(2.1)$$

where $i0$ in the denominator stands for a pure imaginary infinitesimal with a positive imaginary part, e and m are the electron charge and mass, respectively, $\hbar$ is the Planck constant, ρ_T is the volume density of nanotubes, $\hat{p}_i$ is the electron momentum, and f is the Fermi distribution function: $f(E)=1/\{\exp[\beta(E-\mu)]+1\}$ with inverse temperature β and chemical potential μ. For the half-filled case, which we are interested in, $\mu=0$.

The $\mathbf{k}$-linear terms of $\bar{\epsilon}_{ij}(\mathbf{k},\omega)$ are specified by its derivatives with respect to the lth component of the wave vector $\mathbf{k}$. We divide them into γ_{ijl}^A and γ_{ijl}^S, which are, respectively, antisymmetric and symmetric in the subscripts (j,l):

$$\left.\frac{\partial\bar{\epsilon}_{ij}(\mathbf{k},\omega)}{\partial k_l}\right|_{\mathbf{k}=0}\equiv i\{\gamma_{ijl}^A+\gamma_{ijl}^S\}.$$

Recall that the long-wavelength limit of the dielectric function ϵ_{ij} is obtained from the coefficient of the average polarization $4\pi\langle\mathbf{P}\rangle$ to the field strength $\mathbf{E}_0$ by neglecting the electron coordinate $\hat{\mathbf{r}}$ in the applied field: $\mathbf{E}_0\exp[i\mathbf{k}\cdot(\mathbf{R}+\hat{\mathbf{r}})-i\omega t]\simeq\mathbf{E}_0\exp(i\mathbf{k}\cdot\mathbf{R}-i\omega t)$, where $\mathbf{R}$ stands for the center-of-mass coordinate of the nanotube. Similarly, the sum of the third-rank tensors $i\{\gamma_{ijl}^A+\gamma_{ijl}^S\}$ is obtained as the coefficient of the average polarization $4\pi\langle P_i\rangle$ to the product k_lE_{0j} by replacing the applied field to its first-order correction with respect to the electron coordinates: $i(\mathbf{k}\cdot\hat{\mathbf{r}})\mathbf{E}_0\exp(i\mathbf{k}\cdot\mathbf{R}-i\omega t)$. This replacement corresponds to the substitution of

$$i\{(\mathbf{k}\cdot\mathbf{r})\hat{p}_j+\text{H.c.}\}=i\sum_l\left\{\sum_\lambda\epsilon_{lj\lambda}\hat{L}_\lambda+\hat{Q}_{jl}\right\}k_l$$

in place of $\hat{p}_j$ in Eq. (2.1), where $\epsilon_{lj\lambda}$ is the alternating tensor of third rank, $\hat{L}_\lambda$ the λth component of the angular-momentum operator, and $\hat{Q}_{jl}\equiv\{\hat{x}_l\hat{p}_j+\hat{x}_j\hat{p}_l+\text{H.c.}\}/2$ the

symmetric tensor with $\hat{x}_l$ the lth component of $\hat{\mathbf{r}}$. Thus the antisymmetric third-rank tensor γ_{ijl}^A is given by

$$\gamma_{ijl}^A=\sum_\lambda\epsilon_{lj\lambda}\frac{4\pi e^2\hbar}{m^2\omega}\rho_T\sum_{\tau,\tau'=\pm}\sum_{N,N'}\int dk$$
$$\times\int dk'\frac{\langle N'k'\tau'|\hat{p}_i|Nk\tau\rangle\langle Nk\tau|\hat{L}_\lambda|N'k'\tau'\rangle}{E_{\tau'}(N',k')-E_\tau(N,k)+\hbar\omega+i0}$$
$$\times\frac{f(E_{\tau'}(N',k'))-f(E_\tau(N,k))}{E_{\tau'}(N',k')-E_\tau(N,k)}\qquad(2.2)$$

and the symmetric one γ_{ijl}^S is obtained from Eq. (2.2) by replacing $\Sigma_\lambda\epsilon_{lj\lambda}\hat{L}_\lambda$ by $\hat{Q}_{jl}$. Expression (2.2) corresponds to Rosenfeld's formula for the rotatory strength of molecules.

The matrix elements of the momentum operator can be estimated as the derivative of the corresponding matrix elements of the Hamiltonian with respect to the wave vector.[18,19,30] However, such a method is not available for the matrix elements of the angular momentum $\hat{\mathbf{L}}$ and quadratic moment $\hat{Q}$. So we directly estimate the matrix elements in a way similar to the first-principle calculation.[20] First we note that since the Bloch state $|Nk\tau\rangle$ is a superposition of the states $|j\rangle$ localized at the jth site, $|Nk\tau\rangle=\Sigma_j g_j(N,k,\tau)|j\rangle$, the matrix element $\langle Nk\tau|\hat{O}|N'k'\tau'\rangle$ in Eqs. (2.1) and (2.2) ($\hat{O}=\hat{p}_j$, $\hat{L}_\lambda$, or $\hat{Q}_{jl}$) is expanded as

$$\langle Nk\tau|\hat{O}|N'k'\tau'\rangle=\sum_{j,j'}g_j^*(N,k,\tau)g_{j'}(N',k',\tau')\langle j|\hat{O}|j'\rangle.\qquad(2.3)$$

As will be outlined in Appendixes A and B, the sum (2.3) can be calculated with the aid of the symmetry argument by White, Robertson, and Mintmire.[14] Along with the line of thought that leads to the π-band energy (1.1), we estimate the response functions under the following assumptions.

(i) The sum (2.3) is well approximated only by the contributions from the on-site and nearest-neighbor pairs.

(ii) The localized state $|j\rangle$ is well described by a superposition of $2p$ Slater orbits for carbon atoms with their axes perpendicular to the tubule surface:

$$|j\rangle=N_j\left\{|\psi_j^{(2p)}\rangle+\sum_k c_{jk}|\psi_k^{(2p)}\rangle\right\},\qquad(2.4)$$

where the leading $2p$ Slater orbit $|\psi_j^{(2p)}\rangle$ is placed at the site j, the summation in the second term runs over the nearest-neighbor sites, and the coefficients c_{jk} are chosen such that $|j\rangle$ is approximately orthogonal to the other localized states (for more details see Appendix C).

The consistency of these assumptions with earlier works[18-20] will be discussed in Sec. III. For details of the calculations see Appendixes A–C. We then obtain

$$\epsilon_{ij}=\epsilon_\parallel e_{zi}e_{zj}+\epsilon_{0\perp}[\delta_{ij}-e_{zi}e_{zj}],\qquad(2.5)$$

$$\sum_l k_l \{\gamma^A_{ijl} + \gamma^S_{ijl}\} = \gamma_{0\parallel} e_{zi}(\mathbf{e}_z \times \mathbf{k})_j + \gamma^{(1)}_\perp (\mathbf{e}_z \times \mathbf{k})_i e_{zj} + \gamma^{(2)}_\perp$$

$$\times \{k_i e_{zj} - \delta_{ij}(\mathbf{k} \cdot \mathbf{e}_z)\} - \zeta_\parallel (\mathbf{k} \cdot \mathbf{e}_z) e_{zi} e_{zj}$$

$$- \zeta_\perp (\mathbf{k} \cdot \mathbf{e}_z)\{\delta_{ij} - e_{zi} e_{zj}\}, \qquad (2.6)$$

where $\mathbf{e}_z$ is the unit vector along the tubule axis [its direction is identical to that of the lattice vector $-(a+2b)\mathbf{x}+(2a+b)\mathbf{y}$], e_{zi} is its ith component, δ_{ij} is the Kronecker delta, and $\mathbf{k}$ and k_l stand for the wave vector and its lth component, respectively. The explicit expressions of the dielectric functions $\epsilon_\parallel$ and $\epsilon_{0\perp}$ and those of the coefficients $\gamma_{0\parallel}$ and $\gamma^{(1)}_\perp$ are given, respectively, in Secs. III and IV, and that of $\gamma^{(2)}_\perp$ is in Appendix C. The subscript 0 in $\epsilon_{0\perp}$ and $\gamma_{0\parallel}$ implies that they are ''bare'' quantities. By comparing Eq. (2.5) with Eq. (2.6), we see that the last two terms of Eq. (2.6) gives a correction with relative order of $\zeta_\alpha |\mathbf{k}| / \epsilon_\alpha \sim$ (interatomic distance)/(wavelength of light) to the dielectric function ϵ_α. In the energy range we are interested in (up to 10 eV), the correction is at most $10^{-3} \epsilon_\alpha$ and thus will be neglected.

Because a nanotube is a cylinder, we have to take into account the depolarization effect. As discussed by Ajiki and Ando,[18] the effective field $\mathbf{E}^{\text{eff}}_\parallel$ parallel to the tubule axis is identical to the applied field $\mathbf{E}_\parallel$ and the effective field $\mathbf{E}^{\text{eff}}_\perp$ perpendicular to the tubule axis is different from the applied field $\mathbf{E}_\perp$ by a factor of $\{1 + 4\pi i \bar{\sigma}_\perp / D\omega\}^{-1}$, where $D = |\mathbf{R}_{ab}|/\pi$ is the diameter of the nanotube and $\bar{\sigma}_\perp$ stands for the surface conductivity along the peripheral direction. On the other hand, when one neglects the depolarization effect, the surface conductivity $\bar{\sigma}_\perp$ gives the perpendicular polarization of $iS\bar{\sigma}_\perp/2\omega$ for a tube with surface area S, which is equal to the polarizability per tube calculated via the linear response theory: $iS\bar{\sigma}_\perp/2\omega = (\epsilon_{0\perp}-1)/4\pi\rho_T = \sqrt{3}S(\epsilon_{0\perp}-1)/4\pi\ell^2\rho_C$, with ρ_C the density of carbon atoms per volume. Thus the total effective field experienced by the tubule is

$$\mathbf{E}^{\text{eff}} \equiv \mathbf{E}^{\text{eff}}_\parallel + \mathbf{E}^{\text{eff}}_\perp = (\mathbf{E} \cdot \mathbf{e}_z)\mathbf{e}_z + \left\{1 + \frac{2\sqrt{3}(\epsilon_{0\perp}-1)}{\rho_C \ell^2 D}\right\}^{-1}$$

$$\times [\mathbf{E} - (\mathbf{E} \cdot \mathbf{e}_z)\mathbf{e}_z].$$

By substituting this into

$$D_i - E_i = \sum_j \{\epsilon_{ij} - \delta_{ij}\} E^{\text{eff}}_j + i \sum_{j,l} \{\gamma^A_{ijl} + \gamma^S_{ijl}\} k_l E^{\text{eff}}_j$$

and neglecting the terms that may give small corrections to the dielectric functions $\epsilon_\parallel$ and $\epsilon_{0\perp}$ (cf. the last arguments in the preceding paragraph), one obtains

$$\mathbf{D}(\mathbf{k},\omega) = \epsilon_\parallel [\mathbf{E}(\mathbf{k},\omega) \cdot \mathbf{e}_z]\mathbf{e}_z + \epsilon_\perp \{\mathbf{E}(\mathbf{k},\omega)$$

$$- [\mathbf{E}(\mathbf{k},\omega) \cdot \mathbf{e}_z]\mathbf{e}_z\} + i\gamma_\parallel \{[\mathbf{k} \times \mathbf{E}(\mathbf{k},\omega)] \cdot \mathbf{e}_z\}\mathbf{e}_z$$

$$+ i\gamma^{(1)}_\perp [\mathbf{e}_z \cdot \mathbf{E}(\mathbf{k},\omega)](\mathbf{e}_z \times \mathbf{k})$$

$$+ i\gamma^{(2)}_\perp \{\mathbf{e}_z \times [\mathbf{k} \times \mathbf{E}(\mathbf{k},\omega)]\}, \qquad (2.7)$$

where $\epsilon_\perp$ and $\gamma_\parallel$ are, respectively, the renormalized values of $\epsilon_{0\perp}$ and $\gamma_{0\parallel}$,

$$\epsilon_\perp = 1 + \left\{1 + \frac{2\sqrt{3}(\epsilon_{0\perp}-1)}{\rho_C \ell^2 D}\right\}^{-1}(\epsilon_{0\perp}-1), \quad (2.8a)$$

$$\gamma_\parallel = \left\{1 + \frac{2\sqrt{3}(\epsilon_{0\perp}-1)}{\rho_C \ell^2 D}\right\}^{-1} \gamma_{0\parallel}. \qquad (2.8b)$$

Note that the above renormalization factor does not depend on the carbon density ρ_C. The depolarization effect can also be obtained from the electron-electron Coulomb interaction via the time-dependent Hartree approximation.

Note that formulas (2.1) and (2.2) are still valid for more general case where each carbon atom is described by j atomic-centered basis functions and hence the tubule electronic states by $2j$ sets of bands $|N,k,\tau\rangle$ ($\tau=1,2,\ldots,2j$). In Appendixes A and B the matrix elements in Eqs. (2.1) and (2.2) and the general expressions of the response functions are calculated with the aid of the symmetry argument of Ref. 14. The frequency dependences of the coefficients $\epsilon_\parallel$, $\epsilon_\perp$, $\gamma_\parallel$, and $\gamma^{(1)}_\perp$ will be described in the following sections.

III. DIELECTRIC FUNCTIONS

A. Parallel dielectric function

The dielectric function $\epsilon_\parallel$ of a nanotube (a,b) for the field parallel to the tubule axis consists of the one due to the interband transition $\epsilon^b_\parallel$ and the one from the free carrier (the Drude term) $\epsilon^f_\parallel$:

$$\epsilon^b_\parallel = 1 + \left(\frac{e\hbar^2}{m}\right)^2 \frac{4\rho_C}{a\ell} \sum_N$$

$$\times \int_{-\pi/\ell}^{\pi/\ell} dk \frac{f(E_+(N,k)) - f(E_-(N,k))}{E_+(N,k) - E_-(N,k)}$$

$$\times \frac{[\text{Re } K_0(N,k)]^2}{(\hbar\omega)^2 + i\hbar^2\omega/\tau_r - [E_+(N,k) - E_-(N,k)]^2},$$

$$(3.1)$$

$$\epsilon^f_\parallel = -\frac{(\hbar\omega_{\text{pl}})^2}{\hbar\omega(\hbar\omega + i\hbar/\tau_r)}, \qquad (3.2a)$$

with ω_{pl} the plasma frequency

$$\omega^2_{\text{pl}} = -\left(\frac{e\hbar}{m}\right)^2 \frac{2\rho_C}{a\ell} \sum_N \int_{-\pi/\ell}^{\pi/\ell} dk [\text{Im } K_0(N,k)]^2$$

$$\times \{f'(E_+(N,k)) + f'(E_-(N,k))\}, \qquad (3.2b)$$

where we have introduced a phenomenological relaxation time[18,19,30,31] τ_r. The quantity $K_0(N,k)$ in Eqs. (3.1) and (3.2b) corresponds to the (dimensionless) matrix element of the momentum operator and is given by

$$K_0(N,k) = e^{-i\theta(N,k)} \sum_{\lambda=1}^3 e^{-i\phi_\lambda(N,k)} [J_1 \cos \eta_\lambda + J_2(1 - \cos \eta_\lambda)^2] \xi_\lambda, \qquad (3.3)$$

where $\theta(N,k)$ is the argument of

TABLE I. Auxiliary variables η_λ, ξ_λ, and $\phi_\lambda(N,k)$. The index $\lambda = 1,2,3$ stands for the three nearest neighbors for a given site. The pair ($\eta_\lambda, \xi_\lambda$) stands for the cylindrical coordinate of a nearest neighbor λ measured from the given site. The angle $\phi_\lambda(N,k)$ is the phase difference of the Block wave function for each nearest-neighbor pair.

Variable \ Index λ	1	2	3
η_λ	$\dfrac{-\pi(a+b)}{a^2+ab+b^2}$	$\dfrac{\pi b}{a^2+ab+b^2}$	$\dfrac{\pi a}{a^2+ab+b^2}$
ξ_λ	$\dfrac{-a+b}{3\sqrt{a^2+ab+b^2}}$	$\dfrac{2a+b}{3\sqrt{a^2+ab+b^2}}$	$\dfrac{-a-2b}{3\sqrt{a^2+ab+b^2}}$
$\phi_\lambda(N,k)$	0	kl	$\dfrac{2\pi N}{a} - \dfrac{b}{a} k\ell$

$$\left\{ \exp\left[-i\left(\frac{2\pi N}{a} - \frac{b}{a} k\ell \right) \right] + \exp(-ik\ell) + 1 \right\},$$

the variables $\phi_\lambda(N,k)$, η_λ, and ξ_λ are listed in Table I, and J_1 and J_2 are matrix elements of the momentum operator with respect to two localized states listed in Table II. The subscripts $\lambda = 1$, 2, and 3 correspond to three different nearest-neighbor pairs (cf. Fig. 1). Note that the interband contribution $\epsilon_\parallel^b$ arises from the wave-number-preserving ("vertical") transitions between the bands with same indices, as in the case of bulk semiconductors [cf. Fig. 2(a)].

For the nanotubes (a,b) with $2a+b=3n$, the interband contribution $\epsilon_\parallel^b$ logarithmically diverges for low temperature $\beta \to \infty$ because of the crossing of two metallic bands at the Fermi wave number. Strictly speaking, the divergence is an artifact since an energy gap appears at the Fermi wave number due to the nonzero curvature[10,11] [for metallic nanotubes (a,b) with $2a+b \neq -3b$] or to the spontaneous lattice distortion[21,22] (at very low temperature). Still, the contribution from the vicinity of the Fermi wave number could be large as the above-mentioned gap is very small. We see that it is not the case and this contribution is negligible compared

to the Drude term. Indeed, for $\hbar\omega \gg \hbar v_F \delta k_c \gg \beta^{-1}$ with $v_F = t_0\ell\sqrt{a^2+ab+b^2}/a\hbar$ the Fermi velocity, we have

$$\epsilon_\parallel^b = \bar{\epsilon}_\parallel^b + 2\left(\frac{e\hbar^2}{m}\right)^2 \frac{4\rho_C}{a\ell} \int_{|k-k_F|<\delta k_c}$$

$$\times dk \frac{f(E_+(n,k)) - f(E_-(n,k))}{E_+(n,k) - E_-(n,k)}$$

$$\times \frac{[\mathrm{Re}\, K_0(n,k)]^2}{(\hbar\omega)^2 + i\hbar^2\omega/\tau_r - [E_+(n,k) - E_-(n,k)]^2}$$

$$\simeq \bar{\epsilon}_\parallel^b - \left(\frac{e\hbar}{m}\right)^2 \frac{8\hbar\rho_C}{a\ell v_F} \frac{[\mathrm{Re}\, K_0(n,k_F)]^2}{\hbar\omega(\hbar\omega + i\hbar/\tau_r)} \ln(\beta\delta E_c),$$

(3.4)

where $\bar{\epsilon}_\parallel^{-b}$ is the finite part of the interband dielectric function, δk_c the wave-number cutoff, $k_F = 2\pi/3\ell$ the Fermi wave number, and $\delta E_c \simeq 1.13\hbar v_F \delta k_c$ the cutoff energy. The singular term of Eq. (3.4) gives an additional contribution to the Drude term (3.2), but it is negligible because its relative magnitude to the Drude term is approximately 5×10^{-4} for

TABLE II. Matrix elements of the differential operator ∂_i and of the angular-momentum operator $x_i\partial_j - x_j\partial_i$ with respect to two localized states. The vector from one center to the other is denoted $\mathbf{d}$, which points to the positive x direction. The y and z directions are orthogonal to it. The function φ_h ($h=x,y,z$) stands for the $2p$ Slater orbit with its axis in the h direction, ℓ is $\frac{3}{2}$ times the C-C distance of the graphite sheet, and D is the tubule diameter. The parameter u is given by $u = Z\ell/3a_{\mathrm{Bohr}}$, with Z the effective charge for the carbon $2p$ orbit and a_{Bohr} the Bohr radius.

$$J_1 \equiv -\frac{3\ell}{2N} \int d^3r\, \varphi_y(\mathbf{r}+\mathbf{d})\partial_x\varphi_y(\mathbf{r}) = \frac{-9e^{-u}}{20N} u^2\left(\frac{u^2}{3} + u + 1\right),$$

$$J_2 \equiv \frac{27D^2}{32\ell N}\left[\int d^3r\, \varphi_x(\mathbf{r}+\mathbf{d})\{\partial_x\varphi_x(\mathbf{r}) - \partial_y\varphi_y(\mathbf{r})\} - 2\int d^3r\, \varphi_y(\mathbf{r}+\mathbf{d})\partial_x\varphi_y(\mathbf{r})\right] = \frac{-27D^2e^{-u}}{320\ell^2 N} u^4(u+1),$$

$$J_3 \equiv -\frac{2\ell^2}{D^2N} \int d^3r\, \varphi_y(\mathbf{r}+\mathbf{d})(y\partial_z - z\partial_y)\varphi_z(\mathbf{r}) = \frac{-2\ell^2 e^{-u}}{3D^2N}\left(\frac{u^3}{5} + \frac{6u^2}{5} + 3u + 3\right)$$

$$J_4 \equiv \frac{9}{2N}\left[\int d^3r\, \varphi_y(\mathbf{r}+\mathbf{d})(y\partial_z - z\partial_y)\varphi_z(\mathbf{r}) - \int d^3r\, \varphi_x(\mathbf{r}+\mathbf{d})(x\partial_y - y\partial_x)\varphi_y(\mathbf{r})\right] = \frac{9e^{-u}}{40N} u^2\left(\frac{u^2}{3} + u + 1\right)$$

$$N \equiv 1 - \frac{9}{4}\left\{\int d^3r\, \varphi_y(\mathbf{r}+\mathbf{d})\varphi_y(\mathbf{r})\right\}^2 = 1 - \frac{9e^{-2u}}{4}\left\{1 + u + \frac{2u^2}{5} + \frac{u^3}{15}\right\}^2$$
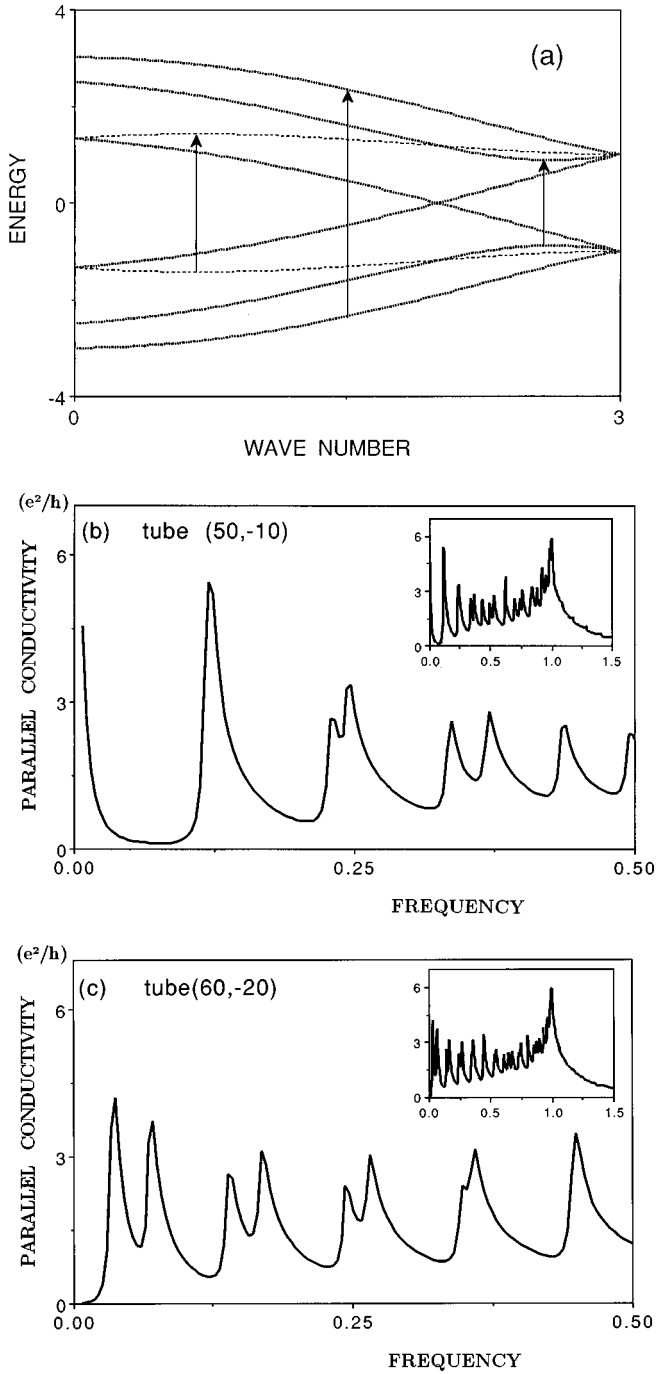
FIG. 2. Real part of the parallel conductivity in unit of e^2/h. (a) Schematic representation of the ''vertical'' transitions responsible for the parallel dielectric function. (b) and (c) Frequency dependence of the real part of the parallel conductivity calculated from the parallel dielectric function as Re $\sigma_\parallel = \omega$ Im $\epsilon_\parallel/4\pi S\rho_T$, with S the area of a single nanotube and ρ_T the tubule density, for (b) a metallic nanotube $(50,-10)$ with a diameter of 3.59 nm and (c) a semiconductive nanotube $(60,-20)$ with a diameter of 4.14 nm. The abscissa represents $\hbar\omega/2t_0$. The insets show the overall views Note that Re $\sigma_\parallel$ does not depend on the carbon density ρ_C.

the nanotube $(5,-1)$ and is less for larger nanotubes.

The frequency dependence of the real part of the parallel conductivity $\sigma_\parallel \equiv -i\omega(\epsilon_\parallel - 1)/4\pi S\rho_T$ for metallic and semiconductive chiral nanotubes are shown respectively in Figs. 2(b) and 2(c) using the parameters listed in Table III. The

growth of the conductivity of the metallic nanotube at low frequency is due to the Drude term (3.2). The low-frequency conductivity ($\hbar\omega/2t_0 \lesssim 0.25$), except for the Drude term, agrees well with the one obtained from the $\mathbf{k}\cdot\mathbf{p}$ model.[18] Indeed, the latter predicts a peak at $\hbar\omega/2t_0 \simeq 3\pi/\sqrt{3(a^2+ab+b^2)}$ for metallic nanotubes of type (a,b) and peaks at $\hbar\omega/2t_0 \simeq \pi/\sqrt{3(a^2+ab+b^2)}$ and $2\pi/\sqrt{3(a^2+ab+b^2)}$ for semiconductive nanotubes. Those correspond to the peak at $\hbar\omega/2t_0 \simeq 0.119$ for the nanotube $(50,-10)$ and to the peaks at $\hbar\omega/2t_0 \simeq 0.034$ and 0.068 for the nanotube $(60,-20)$, which agree well with the present results [cf. Figs. 2(b) and 2(c)].

This can be shown analytically. First, we note that when the tubule radius is large, the dielectric functions (3.1) and (3.2) reduce to the ones obtained within the derivative approximation,[19] except for a numerical factor $(m\ell^2 t_0/\hbar^2 J_1)^2$. Indeed, at absolute zero temperature, one has

$$\left(\frac{m\ell^2 t_0}{\hbar^2 J_1}\right)^2 \{\epsilon_\parallel^b - 1\} = -8\pi e^2\frac{\rho_C\ell}{a}\int\frac{dk}{2\pi}\frac{1}{\hbar\omega_{vc}(N,k)}$$

$$\times\frac{|\hat{v}_{vc}(N,k)|^2}{\omega(\omega+i/\tau_r)-\omega_{vc}(N,k)^2}, \quad (3.5)$$

where $\hbar\omega_{vc}(N,k) = E_+(N,k) - E_-(N,k)$ is the energy difference between the valence and conduction bands and the velocity matrix element $\hat{v}_{vc}(N,k)$ along the tubule axis with respect to the valence and conduction bands is calculated from the wave-number derivative of the Hamiltonian matrix elements.[19,30] Furthermore, when one deals with only the low-energy excitations, the dielectric function (3.5) is well approximated by the contributions from the states near the Fermi points, which are just the ones given by the $\mathbf{k}\cdot\mathbf{p}$ model.[18]

Finally, we compare the present results with the ones obtained by a first-principles local-density-functional (LDF) method.[20] Mintmire and White[20] have reported their calculations on the imaginary parts of the dielectric functions for the nanotube $(5,7)$, which has a diameter of 0.84 nm and is equivalent to the nanotube $(12,-5)$ in our notation. At the energy $\hbar\omega \lesssim 10$ eV, the imaginary part of the parallel dielectric function has a large peak at $\hbar\omega = E_{\text{gap}}^L = 0.86$ eV with a shoulder at $\hbar\omega \simeq 1.7 E_{\text{gap}}^L$ and a smaller peak at $\hbar\omega \simeq 4.4 E_{\text{gap}}^L$. This results can be compared with the one obtained from Eq. (3.1) for $\hbar/\tau_r = 0.3t_0$, which has a large peak at $\hbar\omega = E_{\text{gap}} = 0.35t_0$ with a shoulder at $\hbar\omega \simeq 1.75 E_{\text{gap}}$ and smaller peaks at $\hbar\omega \simeq 4.08 E_{\text{gap}}$ and $5.42 E_{\text{gap}}$. This difference is due to the difference in the calculated band structures. The LDF calculation predicts[20] six local minima in the energy difference between the valence and conduction bands, namely, $E_v - E_c = E_{\text{gap}}^L$, $1.9 E_{\text{gap}}^L$, $3.6 E_{\text{gap}}^L$, $3.9 E_{\text{gap}}^L$, $4.3 E_{\text{gap}}^L$, and $4.5 E_{\text{gap}}^L$. The first two minima correspond to the first peak and the associated shoulder of Im $\epsilon_\parallel$ and the rest to the second peak.[20] On the other hand, the band energy (1.1) gives six local minima $E_v - E_c = E_{\text{gap}}$, $1.92 E_{\text{gap}}$, $3.76 E_{\text{gap}}$, $4.26 E_{\text{gap}}$, $5.48 E_{\text{gap}}$, and $5.55 E_{\text{gap}}$ and the first two minima, middle two minima, and the last two minima generate three peaks in Im $\epsilon_\parallel$. If one uses $t_0 = 2.4$ eV, which is obtained for the nanotube $(5,5)$ by the LDF calculation,[13] instead of $t_0 = 2.7$ eV, we have $E_{\text{gap}} = 0.35t_0 = 0.84$ eV and hence the first

three minima in the energy difference and the first two peaks in Im $\epsilon_\parallel$ obtained respectively from Eqs. (1.1) and (3.1) agree well with the LDF results. At higher energy than $4E_{\mathrm{gap}}^L$ $\simeq 3.4$ eV, a difference appears in both the band structure and Im $\epsilon_\parallel$ because of the tubule curvature. Since the curvature effects become less significant for larger nanotubes, the difference is expected to be very small for nanotubes with diameter more than a few nanometers, which we are mainly interested in.

B. Perpendicular dielectric function

Only the interband transitions contribute to the bare dielectric function $\epsilon_{0\perp}$ of the nanotube (a,b) for the field perpendicular to the tubule axis:

$$\epsilon_{0\perp} = 1 + \left(\frac{e\hbar^2}{\pi m}\right)^2 \frac{\rho_C(a^2+ab+b^2)}{3a\ell} \sum_N \int_{-\pi/\ell}^{\pi/\ell} dk$$

$$\times \frac{f(E_+(N+1,k+\kappa_0)) - f(E_-(N,k))}{E_+(N+1,k+\kappa_0) - E_-(N,k)}$$

$$\times \frac{|K_+(N+1,k+\kappa_0) + K_-^*(N,k)|^2}{(\hbar\omega)^2 + i\hbar^2\omega/\tau_r - [E_+(N+1,k+\kappa_0) - E_-(N,k)]^2},$$

(3.6)

where $\kappa_0 = \pi(a+2b)/\ell(a^2+ab+b^2)$ and, as before, a phenomenological relaxation time τ_r is introduced. As $K_0(N,k)$, $K_\pm(N,k)$ corresponds to the matrix element of the (dimensionless) momentum operator

$$K_\pm(N,k) = \frac{1}{\sqrt{2}} e^{-i\theta(N,k)} \sum_{\lambda=1}^{3} e^{-i\phi_\lambda(N,k)} [J_1(2\cos\eta_\lambda - 1)$$

$$+ J_2(1-\cos\eta_\lambda)^2](1-e^{\pm i\eta_\lambda}). \quad (3.7)$$

Contrarily to the previous case, the perpendicular dielectric function $\epsilon_{0\perp}$ arises from the transitions accompanied by a wave-number change between the bands with different band indices [cf. Fig. 3(a)]. Indeed, if one maps the bands of the nanotubes to the Brillouin zone of the graphite, the change of the band index and wavenumber $(N,k) \rightarrow (N \pm 1, k \pm \kappa_0)$ corresponds to the wave-vector change perpendicular to the tubule axis with magnitude 1/(tubule radius). As discussed in Ref. 18, this is due to the cylindrical shape of the nanotubes: The uniform field perpendicular to the tubule axis corresponds to the sinusoidal field on the tubule surface with period 2π times the tubule radius and thus induces transitions accompanied by the change of the wave vector corresponding to this periodicity. Note that our transition rule $(N,k) \rightarrow (N\pm 1, k\pm\kappa_0)$ and Ajiki and Ando's rule[18] $(N,k) \rightarrow (N\pm 1, k)$ are actually identical. They look different simply because of the difference of the parametrization of the bands (our k is along the inverse lattice vector $\mathbf{K}_y$ for the graphite lattice and Ajiki and Ando's k is along the tube axis).

In Figs. 3(b) and 3(c) we show the real parts of the bare and renormalized "reduced" perpendicular conductivity $\sigma_{0\perp} \equiv -i\omega(\epsilon_{0\perp}-1)/4\pi S\rho_T$ and $\sigma_\perp \equiv -i\omega(\epsilon_\perp -1)/4\pi S\rho_T$, respectively. Note that the reduced conductivities $\sigma_{0\perp}$ and $\sigma_\perp$ are twice the surface conductivity along the
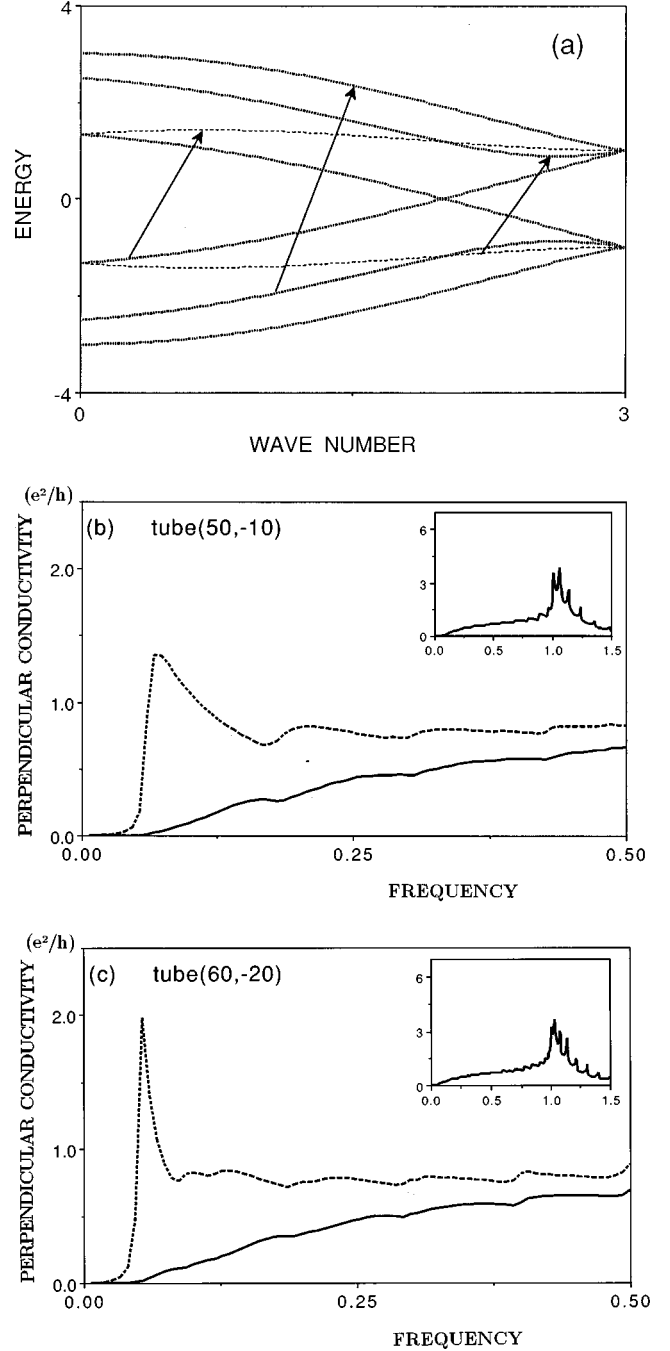

FIG. 3. Real part of the "reduced" perpendicular conductivity in unit of e^2/h. (a) Schematic representation of the transitions responsible for the perpendicular dielectric function. (b) and (c) Frequency dependence of the real part of the perpendicular conductivity calculated from the perpendicular dielectric function via Re $\sigma_\perp = \omega$ Im $\epsilon_\perp/4\pi S\rho_T$ (solid line) and its bare value Re $\sigma_{0\perp} = \omega$ Im $\epsilon_{0\perp}/4\pi S\rho_T$ (broken line), for (b) a metallic nanotube (50, -10) with a diameter of 3.59 nm and (c) a semiconductive nanotube (60,-20) with a diameter of 4.14 nm. The abscissa represents $\hbar\omega/2t_0$. The insets show the overall views of the conductivity with depolarization effect. Note that Re $\sigma_\perp$ does not depend on the carbon density ρ_C.

peripheral direction, but we use these quantities in order to compare the perpendicular dielectric function with the parallel one. We see that the depolarization almost completely smears out the low-frequency resonance peaks. As before,
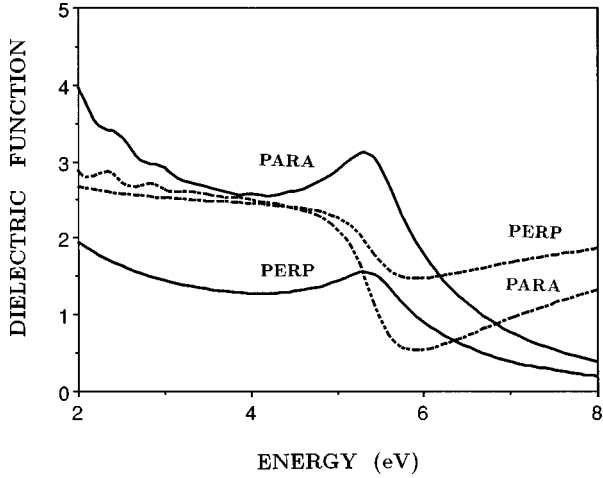
FIG. 4. Dielectric functions for aligned nanotubes $(60, -20)$ with the carbon density 60% of the crystalline graphite. The shorter relaxation time $\hbar/\tau_r = 0.1 \times 2t_0$ is used to simulate the effect of averaging over a tubule size distribution. The bare perpendicular dielectric function is presented instead of the renormalized one since the depolarization effects are suppressed for large nanotubes such as used in the ellipsometry experiment (Ref. 6), with which the present results are compared. The imaginary and real parts of the dielectric functions are shown, respectively, by the solid and broken curves. The curves labeled PARA stand for $\epsilon_\parallel$ and those labeled PERP for $\epsilon_{0\perp}$.

for large nanotubes at low frequency, the present result agrees well with Ajiki and Ando's result. Indeed, when the tubule radius is large and the frequency is low, the perpendicular dielectric function reduces to the one $\epsilon_\perp^{AA}$ obtained by the $\mathbf{k} \cdot \mathbf{p}$ model:[18] $\epsilon_\perp - 1 = \{\hbar^2 J_1 / m\ell^2 t_0\}^2 [\epsilon_\perp^{AA} - 1]$, except for a numerical factor $\{\hbar^2 J_1 / m\ell^2 t_0\}^2$ close to unity. This can also be seen in the figure: Ajiki and Ando's bare perpendicular conductivity for a metallic nanotube has a relatively broad peak at $\hbar\omega / 2t_0 \simeq 1.69\pi / \sqrt{3(a^2 + ab + b^2)}$, which corresponds to a peak at $\hbar\omega / 2t_0 \simeq 0.067$ for the nanotube (50, -10) and thus agrees with the first peak shown in Fig. 3(b). Also, the overall shape of the low-frequency part of Fig. 3(b) including the suppression of peaks is quite similar to that of Ref. 18.

Another remarkable feature of the imaginary parts of the dielectric functions $\mathrm{Im}\epsilon_\parallel$ and $\mathrm{Im}\epsilon_\perp$ is the existence of a relatively broad peak at $\hbar\omega \simeq 2t_0 = 5.4$ eV irrespective of the tubule type. As discussed by Lin and Shung,[19] this feature is consistent with the (5–7)-eV plasmon peak found in the EELS experiments on carbon nanotubes.[7] Also, this result qualitatively agrees with the behavior of the dielectric function observed by de Heer and co-workers[6] for an assembly of aligned nanotubes, where its real and imaginary parts have, respectively, a cutoff and a peak at about 4.6 eV: For such samples, the oscillatory behavior of the dielectric functions is suppressed as a result of averaging over tubules with different sizes. This aspect can be taken into account qualitatively by employing a much shorter relaxation time. In Fig. 4 we show the real and imaginary parts of the dielectric functions $\epsilon_\parallel + \Delta\epsilon$ and $\epsilon_\perp + \Delta\epsilon$ as a function of energy, where the offset dielectric constant $\Delta\epsilon = 1.4$ is the value for graphite,[19] the relaxation time is $\hbar/\tau_r = 0.1 \times 2t_0$, and the other parameters are given in Table III. The result reproduces well the exis-

tence of a peak in the imaginary parts and a cutoff in the real parts at about $\hbar\omega \simeq 2t_0 = 5.4$ eV as well as the difference between the parallel and perpendicular dielectric functions.

C. Drude term

In this subsection we discuss the Drude contribution. As seen from Eq. (3.2b), for large nanotubes at temperatures less than a few hundred kelvin, the plasma frequency ω_{pl} is a function of carbon density ρ_C and tubule diameter D:

$$\omega_{\mathrm{pl}}^2 = \frac{16 J_1^2}{\sqrt{3}\,\pi\ell^2 t_0}\left(\frac{e\hbar}{m}\right)^2 \rho_C \frac{\ell}{D} = \frac{4\pi e^2}{m}\left(0.348 \rho_C \frac{\ell}{D}\right),$$
(3.8)

where the values listed in Table III are used. This behavior can be understood as follows. A nanotube with diameter D has a number of 1D bands, each of which is specified by the quantized wave number along the peripheral direction: $\kappa_\perp = 2\pi s/\pi D$ ($s = 0, 1, \ldots$). The maximum number of the integer s, i.e., the number of 1D bands $\bar{s}$, is given by the condition $\max \kappa_\perp = 2\pi/\ell = 2\pi\bar{s}/\pi D$, which leads to $\bar{s} = \pi D/\ell$. As one of those 1D bands is conductive, $1/\bar{s}$ of the total π electrons behave as free carriers. Thus, because each carbon atom provides one π electron, the free-electron density n_e is given by $n_e = \rho_C/\bar{s} = \rho_C \ell/\pi D$. Substituting this into the well-known formula of the plasma frequency $\omega_{\mathrm{pl}}^2 = 4\pi e^2 n_e/m$, we get

$$\omega_{\mathrm{pl}}^2 = \frac{4\pi e^2}{m}\left(\frac{1}{\pi}\rho_C \frac{\ell}{D}\right),$$

which depends on carbon density and tubule diameter in the same way as our result (3.8). Note that the limiting value $\lim_{D\to\infty} \omega_{\mathrm{pl}} = 0$ correctly corresponds to the plasma frequency of the 2D graphite, which is a gapless semiconductor and has zero plasma frequency.

Now we compare the result with the plasma frequency of an assembly of aligned nanotubes observed by Bommeli et al.[8] Their samples consist of multilayer nanotubes. For such samples, the plasma frequency is given by the average of Eq. (3.8) with respect to a tubule distribution. Here we estimate it by assuming that the assembly is a square lattice of multilayer nanotubes with length $\bar{L}$, outer diameter D_{ex}, and an inner hollow of diameter D_{in}. The density $\rho_C(D)$ of carbon atoms belonging to single-layer tubules with diameter D is $\rho_C(D) = \pi\rho_{GC} D c'/D_{\mathrm{ex}}^2$ since the number of carbon atoms contained in a single-layer tubule of diameter D is $\pi D\bar{L}\sqrt{3}/\ell^2$ and the density of such tubules is $1/D_{\mathrm{ex}}^2\bar{L}$. Here $\rho_{GC} = \sqrt{3}/c'\ell^2 = 0.113$ Å^{-3} is the carbon density of the perfect graphite crystal with $c' = 3.37$ Å the interlayer distance of graphite. Hence

$$\langle \rho_C/D \rangle = \frac{\pi c' \rho_{GC}}{D_{\mathrm{ex}}^2} \times (\text{number of layers in a tubule})$$

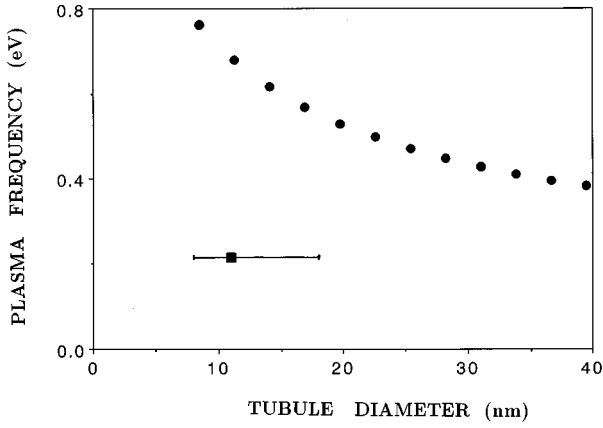$$= \frac{\pi c' \rho_{GC}}{2c''} \frac{D_{\mathrm{ex}} + 2c'' - D_{\mathrm{in}}}{D_{\mathrm{ex}}^2}$$

and

FIG. 5. Diameter dependence of the plasma frequency of randomly synthesized multilayer nanotubes with an inner hollow of diameter $D_{in}=2.2$ nm. A solid square and a horizontal bar indicate the experimental value obtained from the data of Ref. 8 (see the text). The solid square corresponds to the most probable tubule diameter of 11 nm and the horizontal bar (8–18 nm) to the half-width of the tubule-diameter distribution, both for the sample of Ref. 5.

$$(\hbar\omega_{pl})^2 = \frac{16J_1^2}{3\sqrt{3}\,\pi\ell t_0}\left(\frac{e\hbar^2}{m}\right)^2 \frac{\pi c'\rho_{GC}}{2c''}\frac{D_{ex}+2c''-D_{in}}{D_{ex}^2},$$

$$(3.9)$$

where the interlayer distance of $c''=3.4$ Å for a multilayer nanotube and the hollow diameter of $D_{in}=22$ Å are taken from Iijima's observation.[1] Also, we have replaced ρ_{GC} in Eq. (3.9) by $\rho_{GC}/3$ since only the metallic tubules contribute to the Drude term and they account for one-third of the randomly synthesized tubules due to the metallic condition $2a+b=3n$. In Fig. 5 we plot the plasma frequency as a function of tubule diameter D_{ex}.

The plasma frequencies $\hbar\omega_\parallel$ and $\hbar\omega_\perp$, respectively, for the parallel and perpendicular polarization with respect to the sample axis reported by Bommeli et al.[8] are

$$\hbar\omega_\parallel=0.14 \text{ eV}, \quad \hbar\omega_\perp=0.115 \text{ eV}. \quad (3.10)$$

Since, in their samples, the angle α between the tubule axis and the sample axis distributes over some range, the Drude contribution to the average dielectric function is given by

$$\bar{\epsilon}_\parallel=\langle\cos^2\alpha\rangle\epsilon_\parallel^f, \quad \bar{\epsilon}_\perp=\tfrac{1}{2}(1-\langle\cos^2\alpha\rangle)\epsilon_\parallel^f. \quad (3.11)$$

Assuming the uniform distribution of α within an interval $0\le\alpha\le\alpha_0$, one has $\langle\cos^2\alpha\rangle=(\cos^2\alpha_0+\cos\alpha_0+1)/3$ and then $(\omega_\perp/\omega_\parallel)^2=\bar{\epsilon}_\parallel/\bar{\epsilon}_\perp=(1/\langle\cos^2\alpha\rangle-1)/2$, which gives $\alpha_0=76.9°$. For this distribution, the mean value $\bar{\alpha}$ and the standard deviation $\delta\alpha$ are, respectively, $\bar{\alpha}\simeq50°$ and $\delta\alpha\simeq13°$. Also, we find

$$\hbar\omega_{pl}^{expt}=\sqrt{(\hbar\omega_\parallel)^2+2(\hbar\omega_\perp)^2}\simeq0.215 \text{ eV}, \quad (3.12)$$

which is, for the multilayer nanotubes, of diameter 8–18 nm.[5] This value is also shown in Fig. 5. Although the observed and calculated plasma frequencies have the same order of magnitude, the calculated one ω_{pl} is about three times larger than the observed one ω_{pl}^{expt}. This discrepancy cannot be explained by simply adjusting the parameters listed in

Table III within a physically reasonable range. For example, $t_0=3$ eV, $D_{in}=5$ nm, and the other parameter values as before give $\omega_{pl}/\omega_{pl}^{expt}\simeq2.5$, which is still large. One possible reason for this discrepancy is the band-structure change due to interlayer and/or intertubule interactions. In the case of graphite, the interlayer interaction changes the free-carrier density from 0 to about 10^{18} cm^{-3} and the similar change is expected for nanotubes. However, since this value is one order smaller than the free-electron density 3.3×10^{19} cm^{-3} obtained from $\hbar\omega_{pl}^{expt}$, the interlayer and/or intertubule interactions might not be a main reason for the difference between the calculated and observed plasma frequencies. Other possible reason may be the low rate of the metallic tubule synthesis. We have assumed the rate to be $\frac{1}{3}$ based on the condition of metallic tubule formation $2a+b=3n$. However, the metallic tubule synthesis seems to be restricted by the matching of hexagonal patterns between two adjacent layers in a multilayer nanotube as well as other experimental conditions, and the rate of synthesizing metallic tubules might be much smaller than $\frac{1}{3}$, which is estimated to be about $\frac{1}{30.5}$ from the present result.

IV. THIRD-RANK TENSOR AND OPTICAL ACTIVITY

A. Optical activity of the nanotube ensemble

As seen from the explicit expressions [see Eqs. (3.1), (3.2), (3.6), (4.3), (4.4), (4.6), and (C7)], the dielectric functions $\epsilon_\parallel, \epsilon_{0\perp}$ of the nanotube (a,b) are the same as those of its mirror image $(a,-a-b)$, and the components of the third-rank tensors $\gamma_{0\parallel}$, $\gamma_\perp^{(1)}$, and $\gamma_\perp^{(2)}$ are opposite:

$$\epsilon_\parallel(a,-a-b)=\epsilon_\parallel(a,b), \quad \epsilon_{0\perp}(a,-a-b)=\epsilon_{0\perp}(a,b),$$

$$\gamma_{0\parallel}(a,-a-b)=-\gamma_{0\parallel}(a,b),$$

$$\gamma_\perp^{(1)}(a,-a-b)=-\gamma_\perp^{(1)}(a,b),$$

$$\gamma_\perp^{(2)}(a,-a-b)=-\gamma_\perp^{(2)}(a,b).$$

It is also the case for the renormalized quantities $\epsilon_\perp$ and $\gamma_\parallel$. Therefore, the parts of the linear relation (2.7) containing $\gamma_\parallel$ and $\gamma_\perp^{(j)}$ $(j=1,2)$ are responsible for the optical activity of the chiral nanotube. To see it more concretely, we consider the propagation of the light through a film of nanotubes (a,b) with their axes distributed randomly.

By averaging Eq. (2.7) with respect to the direction of $\mathbf{e}_z$, we have

TABLE III. Numerical values of the parameters used to draw the figures.

l (Å)	Z	t_0 (eV)	$\hbar/\tau_r$ (ev)
2.13[a]	3.136[b]	2.7[c]	0.03[d]

[a]Three-halves of the in-plane C-C distance of the graphite.

[b]The ''best atom'' effective charge for carbon in units of e for the 2p Slater orbital (Ref. 32).

[c]The value obtained for $2d$ graphite by a local-density-functional method (Ref. 33).

[d]The value for graphite from Ref. 31.

$$\mathbf{D}(\mathbf{k},\omega) = \frac{\epsilon_\parallel}{2}\{\mathbf{E}(\mathbf{k},\omega) - [\mathbf{E}(\mathbf{k},\omega)\cdot\mathbf{s}]\mathbf{s}\} + \frac{\epsilon_\perp}{2}\{\mathbf{E}(\mathbf{k},\omega)$$

$$+ [\mathbf{E}(\mathbf{k},\omega)\cdot\mathbf{s}]\mathbf{s}\} + i\,\frac{\gamma_\parallel - \gamma_\perp^{(1)}}{2}\,\mathbf{k}\times\mathbf{E}(\mathbf{k},\omega)$$

$$- i\,\frac{\gamma_\parallel}{2}\{[\mathbf{k}\times\mathbf{E}(\mathbf{k},\omega)]\cdot\mathbf{s}\}\mathbf{s}$$

$$- i\,\frac{\gamma_\perp^{(1)}}{2}\,[\mathbf{s}\cdot\mathbf{E}(\mathbf{k},\omega)]\cdot\mathbf{s}\times\mathbf{k}, \qquad (4.1)$$

where $\mathbf{s}$ is the unit normal to the film. From Eq. (4.1) and the Maxwell equations, for the light traveling along the film normal $\mathbf{s}$, the electric field $\mathbf{E}(\mathbf{k},\omega)$ is found to be orthogonal to the wave vector $\mathbf{k}$ and, up to the first order in $\gamma_\parallel$ and $\gamma_\perp^{(1)}$, the complex refractive indices are given by

$$n_\pm = \sqrt{\frac{\epsilon_\parallel + \epsilon_\perp}{2}} \mp \frac{\omega\{\gamma_\parallel - \gamma_\perp^{(1)}\}}{4c},$$

where n_+ and n_- are the refractive indices, respectively, of the right-handed and left-handed circularly polarized lights and c the velocity of light.

As is well known,[28] when the incident light is linearly polarized, the transmitted light is elliptically polarized. For a nanotube film with width d, the angle of rotation of the polarized plane ϕ_r, which measures the strength of the optical rotatory power, and the ellipticity of the polarization of the transmitted light θ_e, which measures the strength of circular dichroism, are give by

$$\phi_r = \frac{d\omega^2}{4c^2}\,\mathrm{Re}\{\gamma_\parallel - \gamma_\perp^{(1)}\}, \quad \theta_e = \frac{d\omega^2}{4c^2}\,\mathrm{Im}\{\gamma_\parallel - \gamma_\perp^{(1)}\}. \qquad (4.2)$$

In the following subsection we study the coefficients $\gamma_\parallel$ and $\gamma_\perp^{(1)}$ in more detail.

B. Third-rank tensor and circular dichroism

As the parallel dielectric function, the bare component $\gamma_{0\parallel}$ of the third-rank tensor for the nanotube (a,b) consists of the interband contribution $\gamma_{0\parallel}^b$ and the free-carrier contribution $\gamma_{0\parallel}^f$,

$$\gamma_{0\parallel}^b = \left(\frac{e\hbar^2}{\pi m}\right)^2 \frac{2\rho_C(a^2 + ab + b^2)}{3a} \sum_N \int_{-\pi/\ell}^{\pi/\ell} dk\,\frac{f(E_+(N,k)) - f(E_-(N,k))}{E_+(N,k) - E_-(N,k)}\,\frac{\mathrm{Re}\,K_0(N,k)\,\mathrm{Re}\,L_0(N,k)}{(\hbar\omega)^2 + i\hbar^2\omega/\tau_r - [E_+(N,k) - E_-(N,k)]^2}, \qquad (4.3)$$

$$\gamma_{0\parallel}^f = \left(\frac{e\hbar^2}{\pi m}\right)^2 \frac{\rho_C(a^2 + ab + b^2)}{3a\hbar\omega(\hbar\omega + i\hbar/\tau_r)} \sum_N \int_{-\pi/\ell}^{\pi/\ell} dk\,\mathrm{Im}\,K_0(N,k)\,\mathrm{Im}\,L_0(N,k)\{f'(E_+(N,k)) + f'(E_-(N,k))\}, \qquad (4.4)$$

where the phenomenological relaxation time τ_r is introduced as before and $L_0(N,k)$ corresponds to the matrix element of the magnetic dipole moment,

$$L_0(N,k) = e^{-i\theta(N,k)} \sum_{\lambda=1}^{3} e^{-i\phi_\lambda(N,k)} \sin\,\eta_\lambda[J_1(2\cos\,\eta_\lambda - 1) + J_2(1 - \cos\,\eta_\lambda)^2 + 2J_3 + 2J_4(1 - \cos\,\eta_\lambda)], \qquad (4.5)$$

with J_3 and J_4 the (dimensionless) matrix elements of the magnetic dipole moment with respect to two localized states listed in Table II. As the perpendicular dielectric function, the other component $\gamma_\perp^{(1)}$ arises from the interband transitions accompanied by the wave-number change,

$$\gamma_\perp^{(1)} = \left(\frac{e\hbar^2}{\pi m}\right)^2 \frac{\rho_C(a^2 + ab + b^2)}{6\sqrt{2}a} \sum_N \int_{-\pi/\ell}^{\pi/\ell} dk\,\frac{f(E_+(N+1,k+\kappa_0)) - f(E_-(N,k))}{E_+(N+1,k+\kappa_0) - E_-(N,k)}$$

$$\times\frac{\mathrm{Im}\{[K_+^*(N+1,k+\kappa_0) + K_-(N,k)][L_-^*(N,k) + L_+(N+1,k+\kappa_0)]\}}{(\hbar\omega)^2 + i\hbar^2\omega/\tau_r - [E_+(N+1,k+\kappa_0) - E_-(N,k)]^2}, \qquad (4.6)$$

where $L_\pm(N,k)$ corresponds to the matrix element of some component of the operator $[\hat{r}_i\hat{p}_j + \hat{p}_j\hat{r}_i]$,

$$L_\pm(N,k) = e^{-i\theta(N,k)} \sum_{\lambda=1}^{3} e^{-i\phi_\lambda(N,k)}\xi_\lambda\{[J_1\cos\,\eta_\lambda$$

$$+ J_2(1 - \cos\,\eta_\lambda)^2](1 + e^{\pm i\eta_\lambda})$$

$$\pm 2iJ_4\sin\,\eta_\lambda(1 - e^{\pm i\eta_\lambda})\}. \qquad (4.7)$$

As in the case of $\epsilon_\parallel^b$, for the half-filled metallic nanotubes, the interband contribution $\gamma_\parallel^b$ may become very large at low temperature $\beta\to\infty$ [cf. the arguments above Eq. (3.4)]. However, actually, it is negligibly small because the ratio of the singular term to the typical peak value of $\gamma_\parallel$ at room temperature is 10^{-4} for nanotube $(5,-1)$ and is less for larger ones.

The frequency dependences of $\mathrm{Re}(\omega\gamma_\parallel/c)$ and $\mathrm{Re}(\omega\gamma_\perp^{(1)}/c)$

are shown respectively in Figs. 6 and 7. They oscillate with a pitch corresponding to the band gap between adjacent bands. Their imaginary parts $\text{Im}(\omega\gamma_\parallel/c)$ and $\text{Im}(\omega\gamma_\perp^{(1)}/c)$ have similar frequency dependences. We also show the bare quantity $\text{Re}(\omega\gamma_{0\parallel}/c)$ in Fig. 6 and find that the effect of depolarization is not significant compared to the perpendicular dielectric function. In contrast to the dielectric functions, the quantities $\gamma_\parallel$ and $\gamma_\perp^{(1)}$ do not exhibit low-energy peaks. This can be understood as follows. As seen in Sec. III, the low-energy peaks come from the transitions between bands near the Fermi energy, which are well described by the $\mathbf{k}\cdot\mathbf{p}$ model.[15,16,18,24] However, it does not distinguish nanotubes from their mirror images. Indeed, the tubule parameters in the $\mathbf{k}\cdot\mathbf{p}$ model are the tubule diameter D and an index ν distinguishing the metallic ($\nu=0$) and semiconductive ($\nu=\pm1$) cases. For example, the nanotube $(5,-1)$ and its mirror image $(5,-4)$ have the same diameter and the index $\nu=0$, but are different. Therefore, in the frequency range where the $\mathbf{k}\cdot\mathbf{p}$ model works well, the nanotubes show no optical activity. Also, this can be checked directly. As an example, the component $\gamma_{0\parallel}^b$ will be considered. Let δE_c be a width of the energy shell near the Fermi energy within which the energy dispersion is well approximated by a linear function of the wave numbers. Then, for low energy $\hbar\omega \le \delta E_c$, because of the factor $1/\{\hbar\omega(\hbar\omega+i\hbar/\tau_r) -4E_+^2(N,k)\}$, the integrand of $\gamma_{0\parallel}$ at energy $|E_\pm(N,k)| \le \delta E_c$ is larger than the rest by a factor of $\hbar/\tau_r\delta E_c$. Hence Eq. (4.3) can be evaluated as

$$\delta_{0\parallel}^b = -2\left(\frac{e\hbar^2}{m}\right)^2 \frac{J_1^2\mathscr{\ell}\rho_C}{\sqrt{3}\pi t_0} \sum_N{}' \int_{-\delta\kappa_C}^{\delta\kappa_C'} d\kappa_\parallel \frac{\kappa_\perp(N)\kappa_\parallel}{\{\kappa_\perp(N)^2+\kappa_\parallel^2\}^{3/2}}$$
$$\times \frac{f_+(N,\kappa_\parallel)-f_-(N,\kappa_\parallel)}{(\hbar\omega)^2+i\hbar^2\omega/\tau_r-4t_0^2[\kappa_\perp(N)^2+\kappa_\parallel^2]}$$
$$+ O(\hbar/\tau_r\delta E_c), \tag{4.8}$$

where $f_\pm(N,\kappa_\parallel) \equiv f(\pm t_0\sqrt{\kappa_\perp(N)^2+\kappa_\parallel^2})$,

$$\kappa_\perp(N) \equiv \frac{2\mathscr{\ell}}{D}\left(N-\frac{b-a}{3}\right),$$

$$\kappa_\parallel \equiv \frac{1}{\sqrt{3}a}\left\{\frac{3\pi D}{2}\delta k-(a+2b)\kappa_\perp(N)\right\},$$

with δk the deviation of k from the Fermi wave number $k_F=2\pi/3\mathscr{\ell}$, the cutoffs of the integral $\delta\kappa_C \sim \delta\kappa_C' \sim \delta E_c/t_0$, and the N-summation running over the bands that pass the vicinity of the Fermi energy E_F; $|E-E_F| \le \delta E_c$. The error introduced by replacing the interval of integration $[-\delta\kappa_C,\delta\kappa_C']$ by $(-\infty,\infty)$ in Eq. (4.8) is also of order $\hbar/\tau_r\delta E_c$ and the integral over $(-\infty,\infty)$ vanishes as it is an integral of an odd function over a symmetric interval. Hence we have the desired result $\gamma_{0\parallel}^b=O(\hbar/\tau_r\delta E_c)$. Note that this implies that the electrons of large nanotubes near the Fermi energy do not "feel" the chirality.

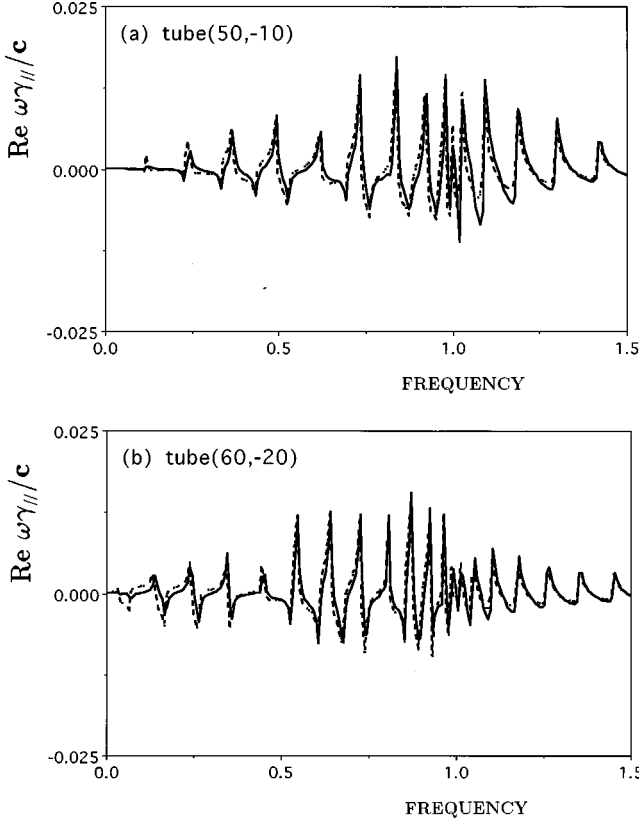

FIG. 6. Frequency dependence of the real part of a dimensionless quantity $\omega\gamma_\parallel/c$. The renormalized quantity $\text{Re}(\omega\gamma_\parallel/c)$ is shown by the solid curve and the bare one $\text{Re}(\omega\gamma_{0\parallel}/c)$ by the broken curve, for (a) a metallic nanotube $(50,-10)$ with a diameter of 3.59 nm and (b) a semiconductive nanotube $(60,-20)$ with a diameter of 4.14 nm. The abscissa represents $\hbar\omega/2t_0$.
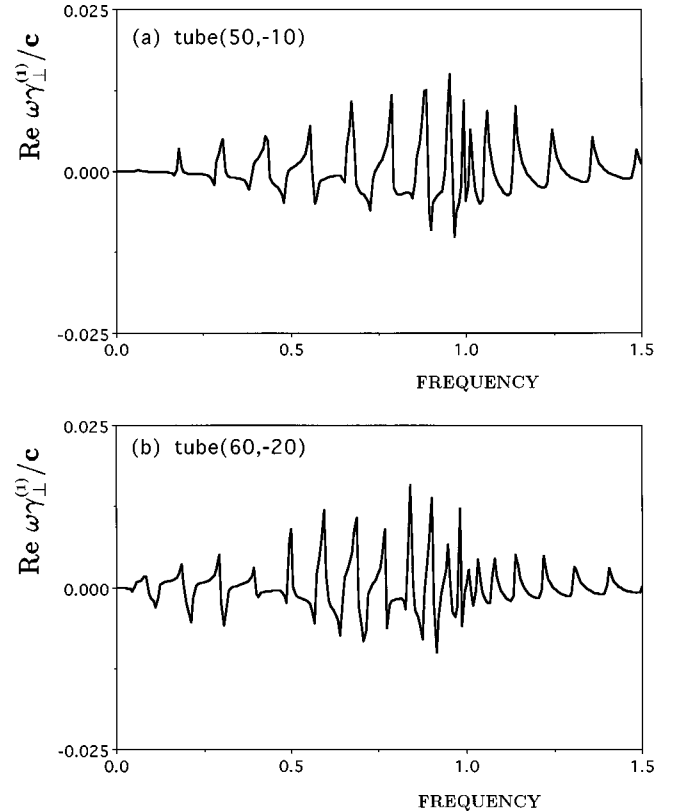

FIG. 7. Frequency dependence of the real part of a dimensionless quantity $\omega\gamma_\perp^{(1)}/c$, for (a) a metallic nanotube $(50,-10)$ with a diameter of 3.59 nm and (b) a semiconductive nanotube $(60,-20)$ with a diameter of 4.14 nm. The abscissa represents $\hbar\omega/2t_0$.

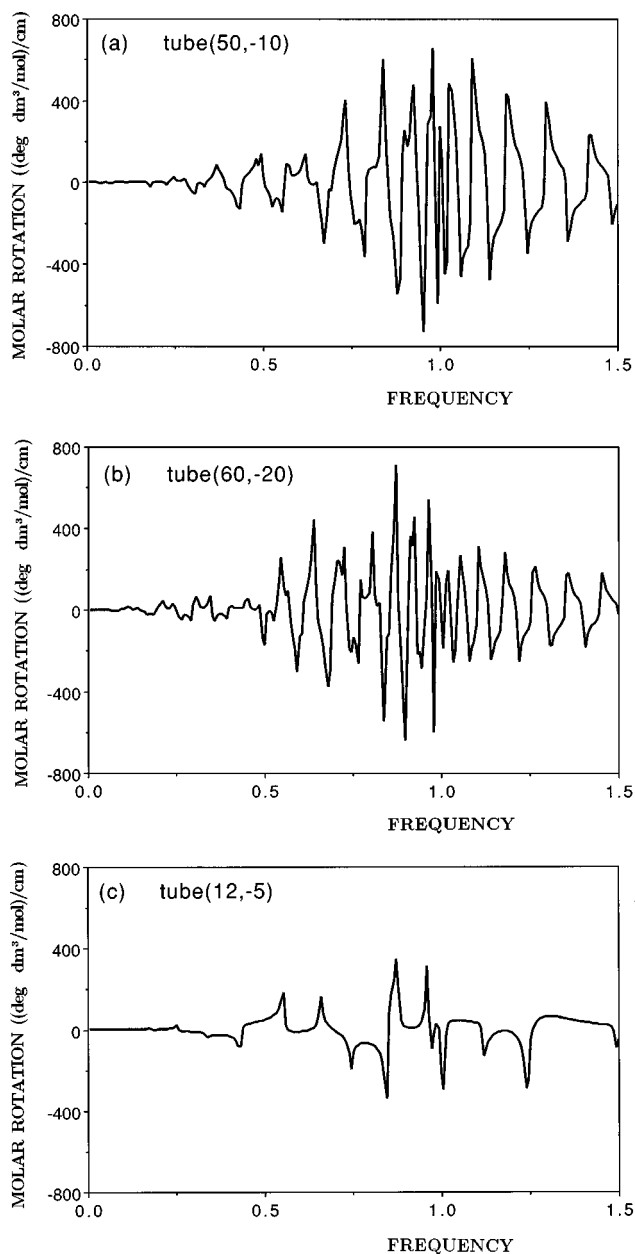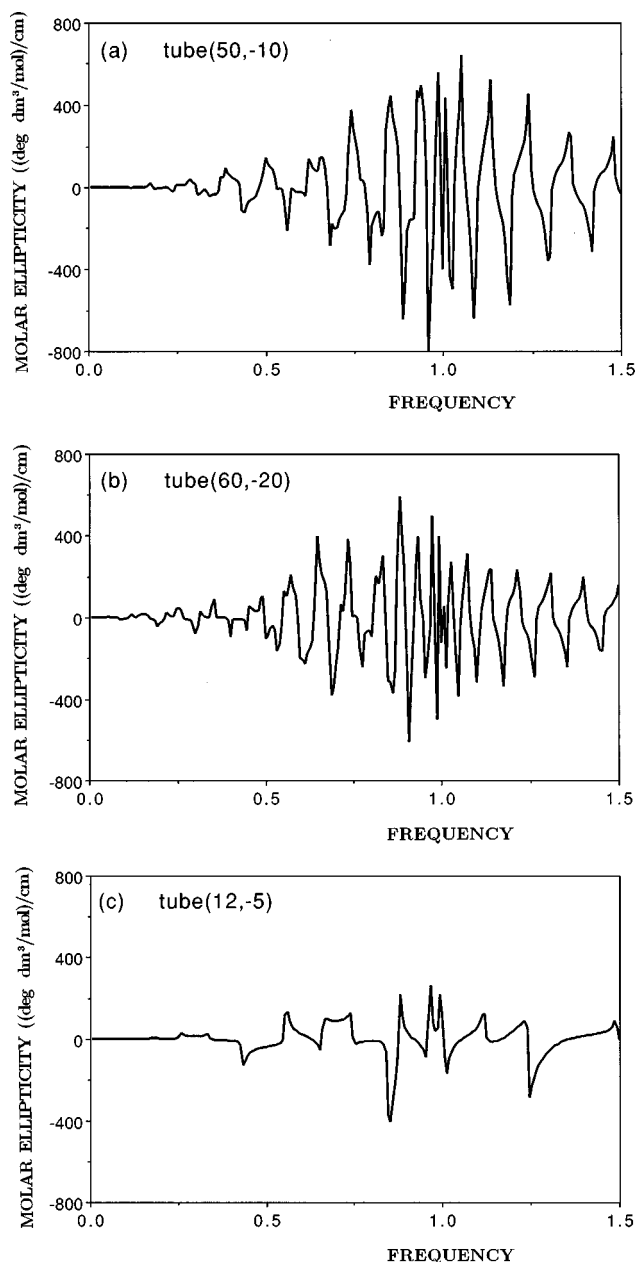FIG. 8. Frequency dependence of the rotation angle for a film of randomly oriented nanotubes with a width of 1 cm and a carbon density of 1 mol/dm^3 for (a) a metallic nanotube $(50,-10)$ with a diameter of 3.59 nm, (b) a semiconductive nanotube $(60,-20)$ with a diameter of 4.14 nm, and (c) a semiconductive nanotube $(12,-5)$ with a diameter of 0.82 nm. The rotation angle is proportional to ω^2 Re$(\gamma_{\parallel} - \gamma)$. The abscissa represents $\hbar\omega/2t_0$

FIG. 9. Frequency dependence of the ellipticity of transmitted light for a film of randomly oriented nanotubes with a width of 1 cm and a carbon density of 1 mol/dm^3 for (a) a metallic nanotube $(50,-10)$ with a diameter of 3.59 nm, (b) a semiconductive nanotube $(60,-20)$ with a diameter of 4.14 nm, and (c) a semiconductive nanotube $(12,-5)$ with a diameter of 0.82 nm. The ellipticity is proportional to ω^2 Im$(\gamma_{\parallel} - \gamma_{\perp}^{(1)})$. The abscissa represents $\hbar\omega/2t_0$.

We show the angle of rotation ϕ_r $[\alpha\omega^2\mathrm{Re}(\gamma_{\parallel} - \gamma_{\perp}^{(1)})]$ of transmitted light in Fig. 8 and the ellipticity θ_e $[\propto \omega^2$ Im $(\gamma_{\parallel} - \gamma_{\perp}^{(1)})]$ in Fig. 9, both of which are given by Eq. (4.2), as a function of frequency. The values correspond to the carbon density of 1 mol/dm$^3 = 6.02 \times 10^{-4}$Å^{-3}, nanotube film width $d = 1$ cm, and the other parameters as listed in Table III. For the nanotube film of 30% density of the graphite crystal, the molar ellipticity $|\theta_e| \simeq 400$ (deg dm^3/mol)/cm corresponds to the difference 6.8 cm^{-1} between the decadic absorption coefficients for the left- and right-handed circularly polarized lights. The value is of the same order of magnitude as those observed in certain organic compounds.[26]

When the frequency of the incident light increases, the negative and positive Cotton effects appear alternately. The pitch of this oscillation corresponds to the band gap between adjacent bands and hence is smaller for larger tubes.

Since the graphite is achiral, the components $\gamma_{\parallel}$, $\gamma_{\perp}^{(1)}$, and $\gamma_{\perp}^{(2)}$ should become smaller for larger tubes. This is indeed the case. The way they disappear can be understood from their oscillatory nature mentioned above: When the tubes are large enough so that the pitch of the oscillation is smaller than the width of each peak, the adjacent peaks in $\gamma_{\parallel}$ with opposite signs cancel each other and $\gamma_{\parallel}$ vanishes. This implies that the optical activity is higher for smaller nano-

tubes and thus may provide a way of detecting small-size nanotubes once the asymmetric synthesis succeeds.

V. SUMMARY AND CONCLUSIONS

Based on the tight-binding model, we have derived the expressions of the dielectric functions and the third-rank tensor responsible for the optical activity and studied their frequency dependences for the half-filled nanotubes. We have shown the following.

(i) The imaginary part of the parallel dielectric function shows peaks at frequencies corresponding to the wave-number-preserving transitions between bands with the same indices. Because of the cylindrical shape of the tube, the peaks of the perpendicular dielectric function come from the wave-number-nonpreserving transitions between the bands with different indices, but its low-frequency peaks are strongly suppressed by depolarization. Both parallel and perpendicular dielectric functions exhibit a plasmon peak at about $\hbar\omega = 2t_0 \simeq 5.4$ eV, which is consistent with the EELS experiments.[7] These results agree well with the previous theoretical works.[18–20] Moreover, the dielectric functions simulated using a very short relaxation time are consistent with the ellipsometry results on aligned multilayer nanotubes by de Heer and co-workers.[6]

(ii) For large nanotubes, the square of the plasma frequency is shown to be proportional to the carbon density and inversely proportional the tube diameter. The calculated value of $\hbar\omega_{pl} \simeq 0.686$ eV for the tubes with a diameter of about 11 nm and an inner hollow of diameter 2.2 nm is of the same order of magnitude as, but three times larger than, the experimental value ($\simeq 0.215$ eV) obtained from the data by Bommeli et al.[8] The reason for this discrepancy is attributed to the lower rate (about $\frac{1}{30.5}$) of the metallic tubule synthesis than that expected from the condition of metallic tubule formation $2a + b = 3n$.

(iii) Chiral nanotubes are optically active. The optical rotatory power and the circular dichroism oscillates as the frequency of the external field increases. Their low-frequency peaks are suppressed since, in this frequency range, the nanotubes are described well by the $\mathbf{k} \cdot \mathbf{p}$ model, which does not describe the chirality.

(iv) For the nanotubes with a diameter of about 4 nm and 30% density of graphite crystal, the optical rotatory power and circular dichroism are found to have peak values of the same order of magnitude as those of certain organic compounds.[26]

(v) The optical activity diminishes for nanotubes with larger diameter D and thus it may provide a way of detecting small-size nanotubes once the asymmetric synthesis succeeds.

In the present work, only the π-band contributions are considered. To obtain more precise information on the optical properties, one should take into account the virtual σ-σ and π-σ transitions since they also contribute to the real parts of the dielectric functions ϵ_{ij} and the third-rank tensor γ_{ijl}. However, such contributions are expected to have no structure and to be nearly constant in the frequency range we are interested in and thus may not affect the qualitative features of the present results.

APPENDIX A: MATRIX ELEMENTS

In this appendix, following the symmetry argument by White, Robertson, and Mintmire,[14] we calculate the matrix elements appearing in the expressions of the response functions (2.1) and (2.2) for the case where each carbon atom is described by j atomic-centered basis functions. First we briefly review the arguments of Ref. 14 in terms of slightly different notations. Since the unit tubule cell consists of two carbon atoms, a basis function $|m, n, \lambda\rangle$ centered on each atom is specified by an orbital label λ ($= 1, 2, \ldots, 2j$) and a tubule cell label (m, n), where the (m, n) tubule cell corresponds to the unit cell in the plane located at $m\mathbf{x} + n\mathbf{y}$ (cf. Fig. 1). Now, as discussed in Ref. 14, the nanotube (a, b) is symmetric with respect to a $2\pi/M$ rotation $\mathcal{C}_M$ around the cylinder axis and a screw operation $\mathcal{S}(h, \alpha)$ representing a translation h units along the cylinder axis in conjunction with an α radian rotation around this axis. In the above, M is the largest common divisor of a and $|b|$, $h \equiv M\ell/\sqrt{a^2 + ab + b^2}$, and $\alpha \equiv \pi\{(2a + b)p_1 + (a + 2b)p_2\}/(a^2 + ab + b^2)$, where a pair of integers (p_1, p_2) ($p_1 > 0$) satisfies $ap_2 - bp_1 = M$ and minimizes $|p_1\mathbf{x} + p_2\mathbf{y}|$. Then two different basis functions $|m, n, \lambda\rangle$ and $|m = 0, n = 0, \lambda\rangle$ are related by those symmetry operations[14]

$$|m, n, \lambda\rangle = \mathcal{C}_M^{\mu(m,n)} \mathcal{S}(h, \alpha)^{\nu(m,n)} |m = 0, n = 0, \lambda\rangle, \quad \text{(A1)}$$

where $\mu(m, n) = p_2 m - p_1 n$ and $\nu(m, n) = (an - bm)/M$. As a result, symmetry-adapted generalized Bloch bases

$$|N, k, \lambda\rangle \equiv \sqrt{\frac{\ell}{2\pi a}} \sum_{m,n,} f_{N,k}(m, n) |m, n, \lambda\rangle, \quad \text{(A2a)}$$

$$f_{N,k}(m, n) \equiv \exp\left\{i\ell\left[\left(\frac{2\pi N}{\ell a} - \frac{b}{a}k\right)m + kn\right]\right\} \quad \text{(A2b)}$$

are simultaneous eigenstates of the two symmetry operations $\mathcal{C}_M$ and $\mathcal{S}(h, \alpha)$, where $N = 0, 1, \ldots, a - 1$ and $k \in [-\pi/\ell, \pi/\ell]$. Also, they block diagonalize the Hamiltonian H:

$$\langle N,k,\lambda|H|N',k',\lambda'\rangle = \delta_{N,N'}\delta(k-k')\sum_{m',n'}f_{N,k}(m',n')$$

$$\times\langle m=0,n=0,\lambda|H|m',n',\lambda'\rangle$$

$$\equiv \delta_{N,N'}\delta(k-k')\mathcal{M}(N,k)_{\lambda,\lambda'}, \quad (A3)$$

where a $2j\times 2j$ matrix $\mathcal{M}(N,k)_{\lambda,\lambda'}$ is introduced. The eigenenergies $E_\tau(N,k)$ ($\tau=1,\ldots,2j$) are eigenvalues of the matrix $\mathcal{M}(N,k)_{\lambda,\lambda'}$ and the corresponding eigenfunctions $|N,k,\tau\rangle$ are superposition of $2j$ generalized Bloch bases

$$|N,k,\tau\rangle = \sum_{\lambda=1}^{2j} b_{\tau\lambda}(N,k)|N,k,\lambda\rangle, \quad (A4)$$

with $b_{\tau\lambda}$ being the coefficients. Note that the energy eigenstates $|N,k,\tau\rangle$ are also the simultaneous eigenstates of the symmetry operations

$$\mathcal{S}(h,\alpha)|N,k,\tau\rangle = \exp\{-i(2\pi Np_1+Mk\ell)/a\}|N,k,\tau\rangle, \quad (A5a)$$

$$\mathcal{C}_M|N,k,\tau\rangle = \exp\{-2\pi iN/M\}|N,k,\tau\rangle. \quad (A5b)$$

As an example, we calculate the matrix element of the angular-momentum component along $\mathbf{e}_\pm$: $\hat{\mathbf{L}}\cdot\mathbf{e}_\pm$, where $\mathbf{e}_\pm=(\mathbf{e}_x\pm i\mathbf{e}_y)/\sqrt{2}$ with $(\mathbf{e}_x,\mathbf{e}_y,\mathbf{e}_z)$ an orthonormal basis set including the unit vector $\mathbf{e}_z$ along the tubule axis. Since $\mathcal{C}_M$ is a rotation and $\mathcal{S}(h,\alpha)$ is a screw operation, both with respect to $\mathbf{e}_z$, we have

$$\mathcal{C}_M^{-1}(\hat{\mathbf{L}}\cdot\mathbf{e}_\pm)\mathcal{C}_M = \exp\left(\pm i\frac{2\pi}{M}\right)(\hat{\mathbf{L}}\cdot\mathbf{e}_\pm), \quad (A6a)$$

$$\mathcal{S}(h,\alpha)^{-1}(\hat{\mathbf{L}}\cdot\mathbf{e}_\pm)\mathcal{S}(h,\alpha) = \exp(\pm i\alpha)\{(\hat{\mathbf{L}}\cdot\mathbf{e}_\pm)\pm i\hbar(\hat{\mathbf{p}}\cdot\mathbf{e}_\pm)\}. \quad (A6b)$$

Using Eq. (A1) and repeatedly applying Eqs. (A6a) and (A6b), we have

$$\langle m,n,\lambda|(\hat{\mathbf{L}}\cdot\mathbf{e}_\pm)|m',n',\lambda'\rangle$$

$$= e^{\pm i[(2\pi/M)\mu+\alpha\nu]}\langle 0,0,\lambda|\{(\hat{\mathbf{L}}\cdot\mathbf{e}_\pm)$$

$$\pm i\nu h(\hat{\mathbf{p}}\cdot\mathbf{e}_\pm)\}|m'-m,n'-n,\lambda'\rangle,$$

where $\mu(m,n)$ and $\nu(m,n)$ are abbreviated, respectively, as μ and ν. Then, because of

$$\frac{2\pi\mu}{M}+\alpha\nu = \ell\left\{\left(\frac{2\pi}{M}-\frac{b}{a}\kappa_0\right)m+\kappa_0 n\right\},$$

$$h\nu = \frac{\ell(na-mb)}{\sqrt{a^2+ab+b^2}},$$

with $\kappa_0\equiv\pi(a+2b)/\{\ell(a^2+ab+b^2)\}$ and the formula

$$\frac{\ell}{2\pi a}\sum_{m,n}f_{N'-N\mp 1,k'-k\mp\kappa_0}(m,n)=\delta_{N',N\pm 1}\delta(k'-k\mp\kappa_0),$$

we obtain

$$\langle N,k,\lambda|(\hat{\mathbf{L}}\cdot\mathbf{e}_\pm)|N',k',\lambda'\rangle = \frac{\ell}{2\pi a}\sum_{m,n,m',n'}f_{N,k}^*(m,n)f_{N',k'}(m'n')\langle m,n,\lambda|(\hat{\mathbf{L}}\cdot\mathbf{e}_\pm)|m',n',\lambda'\rangle$$

$$= \delta_{N',N\mp 1}\delta(k'-k\pm\kappa_0)\sum_{m',n'}f_{N',k'}(m'n')\langle 0,0,\lambda|(\hat{\mathbf{L}}\cdot\mathbf{e}_\pm)|m',n',\lambda'\rangle$$

$$\pm\frac{a\delta_{N',N\mp 1}\delta'(k'-k\pm\kappa_0)}{\sqrt{a^2+ab+b^2}}\sum_{m',n'}f_{N',k'}(m'n')\langle 0,0,\lambda|(\hat{\mathbf{p}}\cdot\mathbf{e}_\pm)|m',n',\lambda'\rangle,$$

where $\delta_{N',N\pm 1}$ is Kronecker's delta and $\delta(k'-k\pm\kappa_0)$ Dirac's delta function. In terms of symmetrized matrix elements

$$\langle\langle N,k,\tau|\hat{O}|N',k',\tau'\rangle\rangle \equiv \frac{1}{2}\sum_{\substack{\lambda,\lambda'\\m,n}}b_{\tau\lambda}^*(N,k)b_{\tau'\lambda'}(N',k')$$

$$\times[f_{N',k'}(m,n)\langle 0,0,\lambda|\hat{O}|m,n,\lambda'\rangle$$

$$+f_{N,k}^*(m,n)\langle m,n,\lambda|\hat{O}|0,0,\lambda'\rangle], \quad (A7)$$

we have

$$\langle N,k,\tau|(\hat{\mathbf{L}}\cdot\mathbf{e}_\pm)|N',k',\tau'\rangle$$

$$= \delta_{N',N\mp 1}\delta(k'-k\pm\kappa_0)\langle\langle N,k,\tau|(\hat{\mathbf{L}}\cdot\mathbf{e}_\pm)|N',k',\tau'\rangle\rangle$$

$$\pm\frac{a\delta_{N',N\mp 1}\delta'(k'-k\pm\kappa_0)}{\sqrt{a^2+ab+b^2}}$$

$$\times\langle\langle N,k,\tau|(\hat{\mathbf{p}}\cdot\mathbf{e}_\pm)|N',k',\tau'\rangle\rangle. \quad (A8)$$

The other matrix elements can be calculated in a similar way. Here we list only the ones necessary in Appendix B:

$$\langle N,k,\tau|(\hat{\mathbf{p}}\cdot\mathbf{e}_z)|N',k',\tau'\rangle = \delta_{N',N}\delta(k'-k)$$

$$\times\langle\langle N,k,\tau|(\hat{\mathbf{p}}\cdot\mathbf{e}_z)|N',k',\tau'\rangle\rangle, \quad (A9a)$$

$$\langle N,k,\tau|(\hat{\mathbf{L}}\cdot\mathbf{e}_z)|N',k',\tau'\rangle = \delta_{N',N}\delta(k'-k)$$

$$\times\langle\langle N,k,\tau|(\hat{\mathbf{L}}\cdot\mathbf{e}_z)|N',k',\tau'\rangle\rangle. \quad (A9b)$$

Before closing this appendix, we show that, as a result of the time-reversal symmetry, there exists a bijective function $\sigma(\tau)$ of the index τ and

$$E_\tau(N,k) = E_{\sigma(\tau)}(a-N,-k), \tag{A10a}$$

$$\langle\langle N,k,\tau|\hat{O}|N',k',\tau'\rangle\rangle = -e^{i(\Theta-\Theta')}\langle\langle a-N,-k,\sigma(\tau)|\hat{O}^\dagger|a \\ -N',-k',\sigma(\tau')\rangle\rangle^*, \tag{A10b}$$

where $\hat{O}$ is $(\hat{\mathbf{p}}\cdot\mathbf{a})$, $(\hat{\mathbf{L}}\cdot\mathbf{a})$, or $(\mathbf{a}\hat{Q}\mathbf{b}) \equiv \Sigma_{i,j}(a_i\hat{Q}_{ij}b_j)$ $(\mathbf{a},\mathbf{b} = \mathbf{e}_\pm,\mathbf{e}_z)$ and the phase $\Theta-\Theta'$ depends only on N, N', k, k', τ, and τ'.

Let $\mathcal{T}$ be the time-reversal operator; then it satisfies[34]

$$\mathcal{T}\alpha = \alpha^*\mathcal{T}, \quad \langle\psi|\mathcal{T}^\dagger\mathcal{T}|\phi\rangle = \langle\phi|\psi\rangle,$$

$$\mathcal{T}\mathcal{P} = -\mathcal{P}\mathcal{T}, \quad \mathcal{T}H = H\mathcal{T}, \tag{A11}$$

where α is an arbitrary complex number, $\mathcal{P}$ is either a momentum $\hat{p}_j$, an angular momentum $\hat{L}_j$, or an electric quadrapole $\hat{Q}_{ij}$, and ψ and ϕ are any pair of wave functions. As a result of Eq. (A11), the wave function $\mathcal{T}|N,k,\tau\rangle$ is an eigenfunction of the Hamiltonian H with eigenenergy $E_\tau(N,k)$. On the other hand, from Eq. (A11) and $\mathcal{C}_M = \exp[2\pi i(\hat{\mathbf{L}}\cdot\mathbf{e}_z)/\hbar M]$, one finds

$$\mathcal{C}_M\mathcal{T}|N,k,\tau\rangle = \mathcal{T}\mathcal{C}_M|N,k,\tau\rangle = \mathcal{T}e^{-2\pi iN/M}|N,k,\tau\rangle \\ = e^{-2\pi i(a-N)/M}\mathcal{T}|N,k,\tau\rangle.$$

Similarly, $\mathcal{T}|N,k,\tau\rangle$ is an eigenfunction of the screw operation $\mathcal{S}(\alpha,h)$ with an eigenvalue $\exp\{-i[2\pi(a-N)p_1 - Mk\ell]/a\}$. Therefore, the state $\mathcal{T}|N,k,\tau\rangle$ must be proportional to one of the energy eigenfunctions $|a-N,-k,\tau'\rangle$ as the states $|a-N,-k,\tau'\rangle$ are generally nondegenerate for each $(a-N,-k)$:

$$\mathcal{T}|N,k,\tau\rangle = e^{i\Theta(N,k,\tau)}|a-N,-k,\sigma(\tau)\rangle, \tag{A12}$$

where $\Theta(N,k,\tau)$ is some phase and τ' is denoted as $\sigma(\tau)$. Since the eigenenergy of the state on the right-hand side is $E_{\sigma(\tau)}(a-N,-k)$, we have Eq. (A10a).

Now we show Eq. (A10b). Let $\hat{O}$ be one of the operators listed after Eq. (A10b); then $\mathcal{T}\hat{O}^\dagger = -\hat{O}\mathcal{T}$ follows from Eq. (A11) and we have

$$\langle N,k,\tau|\hat{O}|N',k',\tau'\rangle$$

$$= \langle N',k',\tau'|\mathcal{T}^\dagger\mathcal{T}\hat{O}^\dagger|N,k,\tau\rangle$$

$$= -\langle N',k',\tau'|\mathcal{T}^\dagger\hat{O}\mathcal{T}|N,k,\tau\rangle$$

$$= -e^{i(\Theta-\Theta')}\langle a-N',-k',\sigma(\tau')|\hat{O}|a-N,-k,\sigma(\tau)\rangle$$

$$= -e^{i(\Theta-\Theta')}\langle a-N,-k,\sigma(\tau)|\hat{O}^\dagger|a-N', \\ -k',\sigma(\tau')\rangle^*,$$

where Θ and Θ' are abbreviations for $\Theta(N,k,\tau)$ and $\Theta(N',k',\tau')$, respectively. Equation (A10b) follows immediately from this relation. Note that relations (A10) guarantee the uniaxial symmetry of the dielectric function ϵ_{ij} with respect to the unit vector $\mathbf{e}_z$.

APPENDIX B: RESPONSE FUNCTIONS (GENERAL CASE)

The response functions can be obtained by a straightforward but tedious calculation. Here we only outline the derivation and give the final results, which are valid for the case where each carbon atom is described by j atomic-centered basis functions.

We consider a component $\Sigma_i e_{zi}\gamma^A_{ijl}$ of the third-rank tensor. It can be rewritten as

$$\sum_i e_{zi}\gamma^A_{ijl} = \sum_\lambda \epsilon_{lj\lambda}\frac{4\pi e^2\hbar^2}{m^2}\rho_T G_\lambda, \tag{B1a}$$

$$G_\lambda = \sum_{\tau,\tau'}\sum_{N,N'}\int dk\int dk'\langle N'k'\tau'|(\hat{\mathbf{p}}\cdot\mathbf{e}_z)|Nk\tau\rangle \\ \times\langle Nk\tau|\hat{L}_\lambda|N'k'\tau'\rangle R(Nk\tau|N'k'\tau'), \tag{B1b}$$

with

$$R(Nk\tau|N'k'\tau') = \frac{1}{\hbar\omega[E_{\tau'}(N',k')-E_\tau(N,k)+\hbar\omega+i0]} \\ \times\frac{f(E_{\tau'}(N',k'))-f(E_\tau(N,k))}{E_{\tau'}(N',k')-E_\tau(N,k)}. \tag{B1c}$$

For notations, see the explanation after Eq. (2.2). Hence Eq. (A9a) gives

$$G_\lambda = \sum_{\tau,\tau'}\sum_N\int dk\langle\langle Nk\tau'|(\hat{\mathbf{p}}\cdot\mathbf{e}_z)|Nk\tau\rangle \\ \times\langle Nk\tau|\hat{L}_\lambda|Nk\tau'\rangle R(Nk\tau|Nk\tau')e_{zi}. \tag{B2}$$

Expanding $\hat{L}_\lambda$ as $\hat{L}_\lambda = (\hat{\mathbf{L}}\cdot\mathbf{e}_z)e_{z\lambda} + (\hat{\mathbf{L}}\cdot\mathbf{e}_+)e_{-\lambda} + (\hat{\mathbf{L}}\cdot\mathbf{e}_-)e_{+\lambda}$ and using Eqs. (A8) and (A9b), we get

$$\langle Nk\tau|\hat{L}_\lambda|N,k,\tau'\rangle = \frac{\ell N_C}{4\pi a}\langle\langle Nk\tau|(\hat{\mathbf{L}}\cdot\mathbf{e}_z)|N,k,\tau'\rangle\rangle e_{z\lambda},$$

where we have used $\delta(0)=\ell N_C/(4\pi a)$ with N_C the number of carbon atoms per tubule. From Eq. (A10) one finds that the function $R(Nk\tau|N'k'\tau')$ in Eq. (B2) can be replaced by

$$\frac{1}{2}[R(Nk\tau|N'k'\tau')+R(N'k'\tau'|Nk\tau)]$$

$$= \frac{1}{(\hbar\omega+i0)^2-[E_\tau(N,k)-E_{\tau'}(N',k')]^2} \\ \times\frac{f(E_{\tau'}(N',k'))-f(E_\tau(N,k))}{E_{\tau'}(N',k')-E_\tau(N,k)}. \tag{B3}$$

A phenomenological relaxation time τ_r is introduced into the response functions by changing $(\hbar\omega+i0)^2$ in Eq. (B3) to $\hbar\omega(\hbar\omega+i\hbar/\tau_r)$. Substituting them into Eq. (B2), one finally obtains

$$\sum_i e_{zi} \gamma^A_{ijl} = \left(\frac{e\hbar}{m}\right)^2 \frac{\ell \rho_C}{a} \sum_\lambda \epsilon_{lj\lambda} e_{z\lambda}$$
$$\times \sum_{\tau,\tau'} \sum_N \int dk \langle\langle Nk\tau'|(\hat{\mathbf{p}}\cdot\mathbf{e}_z)|Nk\tau\rangle\rangle$$
$$\times \langle\langle Nk\tau|(\hat{\mathbf{L}}\cdot\mathbf{e}_z)|Nk\tau'\rangle\rangle G(Nk\tau|Nk\tau'),$$
$$\text{(B4)}$$

where $\rho_C = N_C \rho_T$ is the carbon density and the function G is defined by

$$G(Nk\tau|N'k'\tau')$$
$$\equiv \frac{1}{\hbar\omega(\hbar\omega + i\hbar/\tau_r) - [E_\tau(N,k) - E_{\tau'}(N',k')]^2}$$
$$\times \frac{f(E_{\tau'}(N',k')) - f(E_\tau(N,k))}{E_{\tau'}(N',k') - E_\tau(N,k)}. \quad \text{(B5)}$$

The other components of γ^A_{ijl}, ϵ_{ij}, and γ^S_{ijl} can be calculated in a similar way and we finally obtain

$$\epsilon_{ij} = \epsilon_\| e_{zi} e_{zj} + \epsilon_{0\perp}[\delta_{ij} - e_{zi} e_{zj}], \quad \text{(B6a)}$$

$$\sum_l k_l \{\gamma^A_{ijl} + \gamma^S_{ijl}\} = \gamma_{0\|} e_{zi}(\mathbf{e}_z \times \mathbf{k})_j + \gamma^{(1)}_\perp (\mathbf{e}_z \times \mathbf{k})_i e_{zj}$$
$$+ \gamma^{(2)}_\perp \{k_i e_{zj} - \delta_{ij}(\mathbf{k}\cdot\mathbf{e}_z)\} + \xi_{0\|} e_{zi} k_j$$
$$- \xi_{0\perp}(\mathbf{k}\cdot\mathbf{e}_z)\sum_l \epsilon_{ijl} e_{zl} - \zeta_\|(\mathbf{k}\cdot\mathbf{e}_z) e_{zi} e_{zj}$$
$$- \zeta_\perp(\mathbf{k}\cdot\mathbf{e}_z)\{\delta_{ij} - e_{zi} e_{zj}\}, \quad \text{(B6b)}$$

where the relevant coefficients are given by

$$\epsilon_\| = 1 + \left(\frac{e\hbar}{m}\right)^2 \frac{2\ell\rho_C}{a} \sum_{\tau,\tau'} \sum_N$$
$$\times \int dk |\langle\langle Nk\tau'|(\hat{\mathbf{p}}\cdot\mathbf{e}_z)|Nk\tau\rangle\rangle|^2 G(Nk\tau|Nk\tau'),$$
$$\text{(B7a)}$$

$$\epsilon_{0\perp} = 1 + \left(\frac{e\hbar}{m}\right)^2 \frac{2\ell\rho_C}{a} \sum_{\tau,\tau'} \sum_N \int dk G(Nk\tau|N+1,k$$
$$+ \kappa_0,\tau') |\langle\langle Nk\tau|(\hat{\mathbf{p}}\cdot\mathbf{e}_-)|N+1,k+\kappa_0,\tau'\rangle\rangle|^2,$$
$$\text{(B7b)}$$

and

$$\gamma_{0\|} = \left(\frac{e\hbar}{m}\right)^2 \frac{\ell\rho_C}{a} \sum_{\tau,\tau'} \sum_N \int dk \langle\langle Nk\tau'|(\hat{\mathbf{p}}\cdot\mathbf{e}_z)|Nk\tau\rangle\rangle$$
$$\times \langle\langle Nk\tau|(\hat{\mathbf{L}}\cdot\mathbf{e}_z)|Nk\tau'\rangle\rangle G(Nk\tau|Nk\tau'), \quad \text{(B8a)}$$

$$\gamma^{(1)}_\perp = \left(\frac{e\hbar}{m}\right)^2 \frac{\ell\rho_C}{a} \sum_{\tau,\tau'} \sum_N \int dk \, G(Nk\tau|N+1,k+\kappa_0,\tau')$$
$$\times \text{Im}[\langle\langle N+1,k+\kappa_0,\tau'|(\hat{\mathbf{p}}\cdot\mathbf{e}_+)|Nk\tau\rangle\rangle$$
$$\times \langle\langle Nk\tau|\{(\hat{\mathbf{r}}\cdot\mathbf{e}_-),(\mathbf{p}\cdot\mathbf{e}_z)\}|N+1,k+\kappa_0,\tau'\rangle\rangle], \quad \text{(B8b)}$$

$$\gamma^{(2)}_\perp = \left(\frac{e\hbar}{m}\right)^2 \frac{\ell\rho_C}{a} \sum_{\tau,\tau'} \sum_N \int dk \, G(Nk\tau|N+1,k+\kappa_0,\tau')$$
$$\times \text{Re}[\langle\langle N+1,k+\kappa_0,\tau'|(\hat{\mathbf{p}}\cdot\mathbf{e}_+)|Nk\tau\rangle\rangle$$
$$\times \langle\langle Nk\tau|\{(\hat{\mathbf{r}}\cdot\mathbf{e}_-),(\hat{\mathbf{p}}\cdot\mathbf{e}_z)\}|N+1,k+\kappa_0,\tau'\rangle\rangle], \quad \text{(B8c)}$$

$$\xi_{0\|} = \left(\frac{e\hbar}{m}\right)^2 \frac{\ell\rho_C}{a} \sum_{\tau,\tau'} \sum_N \int dk \langle\langle Nk\tau'|(\hat{\mathbf{p}}\cdot\mathbf{e}_z)|Nk\tau\rangle\rangle$$
$$\times \langle\langle Nk\tau|(\mathbf{e}_+ \hat{Q} \mathbf{e}_-)|Nk\tau'\rangle\rangle G(Nk\tau|Nk\tau'), \quad \text{(B8d)}$$

$$\xi_{0\perp} = \left(\frac{e\hbar}{m}\right)^2 \frac{\ell\rho_C}{a} \sum_{\tau,\tau'} \sum_N \int dk \, G(Nk\tau|N+1,k+\kappa_0,\tau')$$
$$\times \text{Im}[\langle\langle N+1,k+\kappa_0,\tau'|(\hat{\mathbf{p}}\cdot\mathbf{e}_+)|Nk\tau\rangle\rangle$$
$$\times \langle\langle Nk\tau|\{(\hat{\mathbf{r}}\cdot\mathbf{e}_z),(\hat{\mathbf{p}}\cdot\mathbf{e}_-)\}|N+1,k+\kappa_0,\tau'\rangle\rangle]. \quad \text{(B8e)}$$

Note that if the depolarization effect is taken into account as discussed in Sec. II, one obtains

$$\mathbf{D}(\mathbf{k},\omega) = \epsilon_\|[\mathbf{E}(\mathbf{k},\omega)\cdot\mathbf{e}_z]\mathbf{e}_z + \epsilon_\perp\{\mathbf{E}(\mathbf{k},\omega) - [\mathbf{E}(\mathbf{k},\omega)\cdot\mathbf{e}_z]\mathbf{e}_z\}$$
$$+ i\gamma_\|\{[\mathbf{k}\times\mathbf{E}(\mathbf{k},\omega)]\cdot\mathbf{e}_z\}\mathbf{e}_z + i\gamma^{(1)}_\perp[\mathbf{e}_z\cdot\mathbf{E}(\mathbf{k},\omega)]$$
$$\times(\mathbf{e}_z\times\mathbf{k}) + i\gamma^{(2)}_\perp\{\mathbf{e}_z\times[\mathbf{k}\times\mathbf{E}(\mathbf{k},\omega)]\}$$
$$+ i\xi_\|[\mathbf{k}\cdot\mathbf{E}(\mathbf{k},\omega)]\mathbf{e}_z + i\xi_\perp(\mathbf{k}\cdot\mathbf{e}_z)[\mathbf{e}_z\times\mathbf{E}(\mathbf{k},\omega)],$$
$$\text{(B9)}$$

where $\epsilon_\perp$, $\gamma_\|$, $\xi_\|$, and $\xi_\perp$ are, respectively, the renormalized values of $\epsilon_{0\perp}$, $\gamma_{0\|}$, $\xi_{0\|}$, and $\xi_{0\perp}$,

$$\epsilon_\perp = 1 + \left\{1 + \frac{2\sqrt{3}(\epsilon_{0\perp} - 1)}{\rho_C \ell^2 D}\right\}^{-1} (\epsilon_{0\perp} - 1), \quad \text{(B10a)}$$

$$\gamma_\| = \left\{1 + \frac{2\sqrt{3}(\epsilon_{0\perp} - 1)}{\rho_C \ell^2 D}\right\}^{-1} \gamma_{0\|}. \quad \text{(B10b)}$$

$$\xi_\alpha = \left\{1 + \frac{2\sqrt{3}(\epsilon_{0\perp} - 1)}{\rho_C \ell^2 D}\right\}^{-1} \xi_{0\alpha}, \quad \text{(B10c)}$$

with $\alpha = \|$ or $\perp$.

APPENDIX C: RESPONSE FUNCTIONS (π-BAND CONTRIBUTIONS)

Here we outline the derivation of Eqs. (2.5) and (2.6) from Eqs. (B6), (B7), and (B8) under assumptions (i) and (ii) in Sec. II.

1. Localized states

As discussed, the localized state $|j\rangle$ $[j = (m,n,\lambda)]$ is assumed to be well approximated by a superposition

$$|j\rangle = \frac{1}{\sqrt{N_j}} \left\{ |\psi_j^{(2p)}\rangle + \sum_k c_{jk} |\psi_k^{(2p)}\rangle \right\}, \quad \text{(C1)}$$

where $|\psi_j^{(2p)}\rangle$ is the $2p$ Slater orbit of a carbon atom at a position $\mathbf{R}_j$ with its directional vector $\mathbf{c}_j$ perpendicular to the tubule surface:

$$\psi_j^{(2p)}(\mathbf{r}) \propto \mathbf{c}_j \cdot (\mathbf{r} - \mathbf{R}_j) \exp[-Z|\mathbf{r} - \mathbf{R}_j|/(2a_{\mathrm{Bohr}})], \quad \text{(C2)}$$

with Z the effective charge for carbon $2p$ orbit[32] and a_{Bohr} the Bohr radius. In Eq. (C1), N_j is the normalization constant, the k summation runs over the nearest-neighbor sites, and the coefficients c_{jk} will be determined such that the localized state $|j\rangle$ is orthogonal to the other states up to the lowest order in $\epsilon \equiv \exp[-Z\ell/3a_{\mathrm{Bohr}}]$, where ℓ is $\frac{3}{2}$ times the C-C distance.

Let $j = (m, n, \lambda)$ and $k = (m', n', \lambda')$ be nearest-neighbor pairs of lattice sites, then Eq. (C1) gives

$$\langle j|k\rangle = \frac{1}{\sqrt{N_j^* N_k}} \{\langle \psi_j^{(2p)}|\psi_k^{(2p)}\rangle + c_{kj} + c_{jk}^*\} + O(\epsilon^{\sqrt{3}}),$$

whose leading-order term must vanish. Because $\langle \psi_j^{(2p)}|\psi_k^{(2p)}\rangle$ is real and the sites j and k are equivalent, the coefficient c_{jk} is real symmetric. Also, as the coefficients c_{kj} themselves are small, the effects of the tubule curvature can be neglected in $\langle \psi_j^{(2p)}|\psi_k^{(2p)}\rangle$ and one obtains

$$c_{kj} = c_{jk} = -\tfrac{1}{2}\langle \psi_j^{(2p)}|\psi_k^{(2p)}\rangle \simeq c_0$$

$$\equiv -\frac{1}{2} \int d^3\mathbf{r}\, \varphi_y(\mathbf{r}+\mathbf{d}) \varphi_y(\mathbf{r}), \quad \text{(C3)}$$

where φ_y is the $2p$ Slater orbit along the y axis and $\mathbf{d}$ the vector from one site to its nearest-neighbor site, which points in the positive x direction. Then the normalization condition gives

$$\langle j|j\rangle = \frac{1}{N_j}\{1 - 9c_0^2\} + O(\epsilon^{1+\sqrt{3}}) = 1$$

and hence $N_j = 1 - 9c_0^2 + O(\epsilon^{1+\sqrt{3}})$. The so-prepared states $|j\rangle$ satisfy

$$\langle k|j\rangle = \delta_{kj} + O(\epsilon^{\sqrt{3}}). \quad \text{(C4)}$$

In addition, since $\langle u|\hat{O}|u\rangle = 0$ ($\hat{O} = \hat{p}_j,\ \hat{L}_j,$ or $\hat{Q}_{ij}$) for a real wave function $u(\mathbf{r})$, we have

$$\langle j|\hat{O}|j\rangle = 0, \quad \text{(C5a)}$$

$$\langle k|\hat{O}|j\rangle = \frac{\langle \psi_k^{(2p)}|\hat{O}|\psi_j^{(2p)}\rangle}{1 - 9c_0^2} + O(\epsilon^{\sqrt{3}}), \quad \text{(C5b)}$$

where k is one of the nearest neighbors of the site j.

2. Response functions

The symmetrized matrix elements (A7) are evaluated with the aid of Eq. (C5) and one obtains

$$\langle\langle Nk+|(\hat{\mathbf{p}}\cdot\mathbf{e}_z)|N,k,-\rangle\rangle = \frac{\hbar}{i\ell} \operatorname{Re} K_0(N,k), \quad \text{(C6a)}$$

$$\langle\langle N,k,+|(\hat{\mathbf{p}}\cdot\mathbf{e}_z)|Nk+\rangle\rangle = -\langle\langle N,k,-|(\hat{\mathbf{p}}\cdot\mathbf{e}_z)|Nk-\rangle\rangle$$

$$= -\frac{\hbar}{\ell} \operatorname{Im} K_0(N,k), \quad \text{(C6b)}$$

$$\langle\langle N+1,k+\kappa_0,+|(\hat{\mathbf{p}}\cdot\mathbf{e}_+)|Nk-\rangle\rangle$$

$$= \frac{\hbar D}{4i\ell^2} [K_+(N+1,k+\kappa_0)^* + K_-(N,k)], \quad \text{(C6c)}$$

$$\langle\langle N,k,-|(\hat{\mathbf{L}}\cdot\mathbf{e}_z)|Nk+\rangle\rangle = \frac{i\hbar D^2}{4\ell^2} \operatorname{Re} L_0(N,k), \quad \text{(C6d)}$$

$$\langle\langle N,k,+|(\hat{\mathbf{L}}\cdot\mathbf{e}_z)|Nk+\rangle\rangle = -\langle\langle Nk-|(\hat{\mathbf{L}}\cdot\mathbf{e}_z)|Nk-\rangle\rangle$$

$$= -\frac{\hbar D^2}{4\ell^2} \operatorname{Im} L_0(N,k), \quad \text{(C6e)}$$

$$\langle\langle N,k,\tau|(\mathbf{e}_+\hat{Q}\mathbf{e}_-)|Nk\tau'\rangle\rangle = 0, \quad \text{(C6f)}$$

$$\langle\langle Nk-|\{(\hat{\mathbf{r}}\cdot\mathbf{e}_-),(\hat{\mathbf{p}}\cdot\mathbf{e}_z)\}|N+1,k+\kappa_0,+\rangle\rangle$$

$$= \frac{i\hbar D}{4\sqrt{2}\ell} [L_-(N,k)^* + L_+(N+1,k+\kappa_0)], \quad \text{(C6g)}$$

$$\langle\langle Nk-|\{(\hat{\mathbf{r}}\cdot\mathbf{e}_z),(\hat{\mathbf{p}}\cdot\mathbf{e}_-)\}|N+1,k+\kappa_0,+\rangle\rangle$$

$$= -\ell\xi_1\langle\langle N+1,k+\kappa_0,+|(\hat{\mathbf{p}}\cdot\mathbf{e}_+)|Nk-\rangle\rangle^*,$$

$$\text{(C6h)}$$

where D the tubule diameter, $\hbar$ is the Planck constant, the auxiliary quantity ξ_1 is given in Table I, and functions $K_0(Nk)$, $K_\pm(Nk)$, $L_0(Nk)$, and $L_\pm(Nk)$ are defined, respectively, by Eqs. (3.3), (3.7), (4.5), and (4.7).

First, because of Eqs. (C6f) and (C6h), $\xi_{0\perp} = \xi_{0\parallel} = 0$ and thus Eqs. (B6a) and (B6b) reduce to Eqs. (2.5) and (2.6), respectively. Next we consider the other components. We observe that, in the sums in Eq. (B8), two terms corresponding to $(\tau, \tau') = (+, -)$ and $(-, +)$ are identical as a result of the time-reversal symmetry (A10). Also, terms corresponding to $(\tau, \tau') = (+, +)$ and $(-, -)$ do not contribute to $\epsilon_{0\perp}$, $\gamma_\perp^{(1)}$, and $\gamma_\perp^{(2)}$ except at very high temperature because the initial and final states of the matrix elements are simultaneously occupied or unoccupied. Hence $\gamma_\perp^{(2)}$ is given by

$$\gamma_\perp^{(2)} = 2\left(\frac{e\hbar}{m}\right)^2 \frac{\ell\rho_C}{a} \sum_N \int dk\, G(Nk-|N+1,k+\kappa_0,+)$$

$$\times \operatorname{Re}[\langle\langle N+1,k+\kappa_0,+|(\hat{\mathbf{p}}\cdot\mathbf{e}_+)|Nk-\rangle\rangle$$

$$\times \langle\langle Nk-|\{(\hat{\mathbf{r}}\cdot\mathbf{e}_-),(\hat{\mathbf{p}}\cdot\mathbf{e}_z)\}|N+1,k+\kappa_0,+\rangle\rangle]$$

$$= \left(\frac{e\hbar^2}{m}\right)^2 \frac{D^2\rho_C}{8\sqrt{2}\ell^2 a} \sum_N \int dk\, G(Nk-|N+1,k+\kappa_0,+)$$

$$\times \operatorname{Re}\{[K_+(N+1,k+\kappa_0)^* + K_-(N,k)]$$

$$\times [L_+(N+1,k+\kappa_0) + L_-(N,k)^*]\} \quad \text{(C7)}$$

and $\epsilon_{0\perp}$ and $\gamma_{\perp}^{(1)}$ by Eqs. (3.6) and (4.6). The interband contributions to $\epsilon_{\parallel}$ and $\gamma_{\parallel 0}$ are calculated in a similar way and one obtains Eqs. (3.1) and (4.3). The Drude contributions (3.2) to $\epsilon_{\parallel}$ and (4.4) to $\gamma_{0\parallel}$ come from the terms corresponding to $(\tau,\tau')=(+,+)$ and $(-,-)$ with the aid of $G(Nk\tau|Nk\tau)=f'(E_\tau(N,k))/\hbar\omega(\hbar\omega+i\hbar/\tau_r)$.

---

*Present address: Institute of Advanced Energy, Kyoto University, Uji, Kyoto 611, Japan.

[1] S. Iijima, Nature (London) **354**, 56 (1991).

[2] H. Hiura, T. W. Ebbesen, K. Tanigaki, and H. Takahashi, Chem. Phys. Lett. **202**, 509 (1993); K. Tanaka, T. Sato, T. Yamabe, K. Okahara, K. Uchida, M. Yumura, H. Niino, S. Ohshima, Y. Kuriki, K. Yase, and F. Ikazaki, *ibid.* **223**, 65 (1994).

[3] A. P. Ramirez, R. C. Haddon, O. Zhou, R. M. Fleming, J. Zhang, S. M. McClure, and R. E. Smalley, Science **265**, 84 (1994); J. Heremans, C. H. Olk, and D. T. Morelli, Phys. Rev. B **49**, 15 122 (1994); X. K. Wang, R. P. H. Chang, A. Patashinski, and J. B. Ketterson, J. Mater. Res. **9**, 1578 (1994); O. Chauvet, L. Forro, W. Bacsa, D. Ugarte, B. Doudin, and W. A. de Heer, Phys. Rev. B **52**, R6963 (1995).

[4] S. N. Song, X. K. Wang, R. P. H. Chang, and J. B. Ketterson, Phys. Rev. Lett. **72**, 697 (1994); L. Langer, L. Stockman, J. P. Heremans, V. Bayot, C. H. Olk, C. Van Haesendonck, Y. Bruynseraede, and J. P. Issi, J. Mater. Res. **9**, 927 (1994); L. Langer, V. Bayot, J.-P. Issi, L. Stockman, C. Van Haesendonck, Y. Bruynseraede, J. P. Heremans, and C. H. Olk, in *Physics and Chemistry of Fullerenes and Derivatives*, edited by H. Kuzumany *et al.* (World Scientific, Singapore, 1995), p. 565.

[5] W. S. Bacsa, D. Ugarte, A. Chatelain, and W. A. de Heer, Phys. Rev. B **50**, 15 473 (1994).

[6] W. A. de Heer, W. S. Bacsa, A. Chatelain, T. Gerfin, R. Humphrey-Baker, L. Forro, and D. Ugarte, Science **268**, 845 (1995); W. S. Bacsa and W. A. de Heer, in *Physics and Chemistry of Fullerenes and Derivatives* (Ref. 4), p. 574.

[7] R. Kuzuo, M. Terauchi, and M. Tanaka, Jpn. J. Appl. Phys., Part 2 **31**, L1484 (1992); V. P. Dravid, X. Lin, Y. Wang, A. Lee, J. B. Ketterson, and R. P. H. Chang, Science **259**, 1601 (1993); P. M. Ajayan, S. Iijima, and T. Ichihashi, Phys. Rev. B **47**, 6859 (1993); L. A. Bursill, P. A. Stadelmann, J. L. Peng, and S. Prawer, *ibid.* **49**, 2882 (1994); R. Kuzuo, M. Terauchi, M. Tanaka, and Y. Saito, Jpn. J. Appl. Phys., Part 2 **33**, L1316 (1994).

[8] F. Bommeli, L. Degiorgi, P. Wachter, W. S. Bacsa, W. A. de Heer, and L. Forro, Solid State Commun. **99**, 513 (1996).

[9] K. Tanaka, K. Okahara, M. Okada, and T. Yamabe, Chem. Phys. Lett. **191**, 469 (1992).

[10] N. Hamada, S. Sawada, and A. Oshiyama, Phys. Rev. Lett. **68**, 1579 (1992).

[11] R. Saito, M. Fujita, G. Dresselhaus, and M. S. Dresselhaus, Phys. Rev. B **46**, 1804 (1992).

[12] J. W. Mintmire, B. I. Dunlap, and C. T. White, Phys. Rev. Lett. **68**, 631 (1992).

[13] D. H. Robertson, D. W. Brenner, and J. W. Mintmire, Phys. Rev. B **45**, 12 592 (1992).

[14] C. T. White, D. H. Robertson, and J. W. Mintmire, Phys. Rev. B **47**, 5485 (1993).

[15] H. Ajiki and T. Ando, J. Phys. Soc. Jpn. **62**, 1255 (1993); **62**, 2470 (1993); **63**, 4267(E) (1994).

[16] H. Ajiki and T. Ando, J. Phys. Soc. Jpn. **64**, 4382 (1995); Physica B **216**, 358 (1996).

[17] J. P. Lu, Phys. Rev. Lett. **74**, 1123 (1995); H. Ajiki and T. Ando, J. Phys. Soc. Jpn. **65**, 505 (1996).

[18] H. Ajiki and T. Ando, Physica B **201**, 349 (1994); Jpn. J. Appl. Phys., Suppl. **34**, 107 (1995).

[19] M. F. Lin and K. W.-K. Shung, Phys. Rev. B **50**, 17 744 (1994).

[20] J. W. Mintmire and C. T. White, Synth. Met. **77**, 231 (1996).

[21] K. Harigaya, Phys. Rev. B **45**, 12 071 (1992); K. Harigaya and M. Fujita, *ibid.* **47**, 16 563 (1993); Y. Huang, M. Okada, K. Tanaka, and T. Yamabe, Solid State Commun. **97**, 303 (1996).

[22] N. A. Viet, H. Ajiki, and T. Ando, J. Phys. Soc. Jpn. **63**, 3036 (1994); H. Ajiki and T. Ando, *ibid.* **64**, 260 (1995).

[23] M. S. Dresselhaus, G. Dresselhaus, and R. Saito, Carbon **33**, 883 (1995), and references therein.

[24] T. Yamabe, Synth. Met. **70**, 1511 (1995), and references therein.

[25] See, G. S. Painter and D. E. Ellis, Phys. Rev. B **1**, 4747 (1970); C. Fretigny, R. Saito, and H. Kamimura, J. Phys. Soc. Jpn. **58**, 2098 (1989).

[26] See, N. Harada, J. Kohori, H. Uda, K. Nakanishi, and R. Takeda, J. Am. Chem. Soc. **107**, 423 (1985); M. G. Paterlini, T. B. Freedman, and L. A. Nafie, Biopolymers **25**, 1751 (1986).

[27] K. Tanaka, H. Ago, T. Yamabe, K. Okahara, and M. Okada (unpublished); K. Okahara, Ph.D. thesis, Kyoto University, 1994.

[28] L. D. Landau and E. M. Lifshitz, *Electrodynamics of Continuous Media* (Pergamon, Oxford, 1963).

[29] W. A. Harrison, *Electronic Structure and the Properties of Solids* (Freeman, San Francisco, 1980).

[30] L. G. Johnson and G. Dresselhaus, Phys. Rev. B **7**, 2275 (1973).

[31] K. Nakao, J. Phys. Soc. Jpn. **47**, 208 (1979).

[32] B. J. Ransil, Rev. Mod. Phys. **32**, 245 (1960); C. C. J. Roothaan (unpublished).

[33] S. B. Trickey, F. Müller-Plathe, G. H. F. Diercksen, and J. C. Boettger, Phys. Rev. B **45**, 4460 (1992).

[34] E. P. Wigner, *Group Theory and Its Application to the Quantum Mechanics of Atomic Spectra* (Academic, New York, 1959).